Scanning Microscopy

Volume 4 | Number 4 Article 1

9-2-1990

Equations of Charge Distribution in the Environmental Scanning Electron Microscope (ESEM)

G. D. Danilatos
Electroscan Corporation

Scanning Microscopy, Vol. 4, No. 4, 1990 (Pages 799-823) 0891-7035/90$3.00+.00
Scanning Microscopy International, Chicago (AMF O'Hare), IL 60666 USA

EQUATIONS OF CHARGE DISTRIBUTION IN THE ENVIRONMENTAL SCANNING ELECTRON MICROSCOPE (ESEM)

G. D. Danilatos

ESEM Research Laboratory, 98 Brighton Boulevard,
North Bondi (Sydney), N.S.W. 2026, Australia.
and
ELECTROSCAN Corporation, 66 Concord Street,
Wilmington, MA 01887, USA.

(Received for publication February 13, 1990, and in revised form September 2, 1990)

Abstract

In the environmental scanning electron microscope (ESEM), the electron beam together with various signals emanating from the beam-specimen interaction ionize the gaseous medium in the specimen chamber. A detailed derivation of equations describing the charge density and current flow in the system is presented. It is shown that the various causes of ionization operate over distinct regions, which can be separated out by suitable electrode configuration. The electron probe retains a fraction of electrons with the original charge distribution; this is surrounded by a widespread electron skirt, which, in turn, is surrounded by charge created by the secondary electrons, beyond which extends the action of backscattered electrons.

Key words: charge distribution, charge density, environmental scanning electron microscope, gaseous detector, ionization, terminology, specimen current, induction.

Address for correspondence:
ESEM Research Laboratory,
98 Brighton Boulevard,
North Bondi (Sydney),
N.S.W. 2026,
Australia.

Phone No. +61 2 3650326.
FAX No. +61 2 3650326.

Introduction

The environmental scanning electron microscope (ESEM) is a type of SEM that allows the examination of specimens in a gaseous environment. The high vacuum in the electron optics column is separated from the high pressure in the specimen chamber by differential pumping through a system of apertures. The electron beam initially propagates unhindered through the electron optics column until it approaches the final pressure limiting aperture. In the distance from the vicinity of this aperture to the specimen surface, the electron beam loses electrons exponentially. The pressure and travel distance in the specimen chamber can be chosen so that the average number of collisions per electron is below 2 or 3, a condition, which defines the oligo-scattering regime (Danilatos, 1988). It has been shown that in this regime, scanning and probing of the specimen surface can proceed in the usual way. The presence of gas does not deteriorate the resolving power of the instrument, whereas the contrast decreases on account of beam weakening and background noise. However, contrast can be compensated for by an appropriate increase of incident beam current, the quantitative relationships for which have been established in the previous reference.

The distribution of charge around a specimen is much simpler in the vacuum of an SEM than the corresponding distribution in the gaseous conditions of the ESEM. First, the electron beam profile is drastically modified in the ESEM. It has been found (Danilatos, 1988) that, in the oligo-scattering regime, the original beam is split in two fractions, one consisting of the totally unscattered electrons and the other of beam electrons scattered by the gas. The unscattered fraction retains the original electron distribution and, hence, is of the same diameter as the original electron probe, whilst the scattered fraction, referred also as "electron skirt", usually spreads over a radius several orders of magnitude larger than the probe diameter. Second, the important reactions between signals and gas are yet to be explored. This paper concentrates on the reaction between *electrons* and *gas* and, in particular, on the charge generation and distribution (including deposition and collection) from signal-electrons emanating from the beam-specimen interactions and

from electrons emanating from the beam-gas interaction.

This study has been necessitated from the need to understand, design and operate an efficient gaseous detector device (GDD), the fundamentals of which have been presented separately (Danilatos, 1990b). The main purpose of this paper is to present the derivation of equations governing the charge density and current distributions, as they occur in the bulk of the gas and as they are detected by two parallel electrodes defining a uniform electric field. To simplify the basic derivations, the top electrode is a disk with a hole at its center and is positioned at the plane of the final pressure limiting aperture, i.e. it is integrated with the aperture grid. The bottom electrode is a coaxial disk placed at the specimen level and, again for simplicity, is integrated with the specimen. Throughout this work, we will mainly be dealing with two functions of current: (a) The point current density denoted by j(r,D), i.e. the current per unit area at a given point on an electrode at radial distance r from the axis of the system, with D the inter-electrode separation. (b) The disk current I(r,D) derived from the previous function by integration from 0 to radius r. We will examine, in turn, the charge distribution of an electron beam, electron skirt, fast and slow electrons from object in vacuum and in gas, at low and at high electric field. The equations of gaseous gain and charge conservation for the ESEM will also be presented.

Terminology

In the vacuum SEM, we are already faced with a large number of acronyms describing the various signals. For example, we have SE-I (high resolution secondary electrons (SE) produced by the incoming electron beam at the specimen), SE-II (secondary electrons generated by the backscattered electrons (BSE), as they exit from the specimen surface), SE-III (secondary electrons generated by BSE at the pole piece) and SE-IV (secondary electrons generated by the electron beam in the electron optics column) (Peters, 1982). It has been shown by Danilatos (1990b) that the number of types of SE, BSE and photons is greatly increased in the conditions of ESEM. As a result, it would be difficult to memorize all these types by a numerical system, or by addition of a large number of new arbitrary acronyms. An attempt has been made to rationalize a new terminology, a summary of which is given here.

The basic sources, from which signals are produced, are the probe (P), object (O), gas (G), walls (W) and scattered probe (P').

There are three basic types (or carriers) of signals, namely, electrons (E), gaseous ions (I) and rays (R), the latter being all types of photons in the visible and invisible regions.

A further differentiation of signals is according to their energy: For electrons, those having energies less than 50 eV are said to be slow (S), while the others are said to be fast (F). The cascade, or avalanche, electrons appearing in a gaseous discharge are designated as "cascade" (C) electrons. For photons, those in the infra-red, visible and near ultra-violet regions are denoted by the word "light" (L), while the x-rays by X.

An acronym may consist of three letters pertaining to the energy level, the type of carrier and the source of the signal, in that order. Thus, SEO is read as "slow electrons from object", FEO as "fast electrons from object" etc. FEP read as "fast electrons from probe" may be abbreviated to EP, i.e. "electrons from probe", since the probe electrons are only fast ones. CEG read as "cascade electrons from gas" may be abbreviated to CE, i.e. "cascade electrons", since they occur only in the gas (for our purposes in the ESEM).

To complete the system and remove ambiguities, we may combine different acronyms to denote the origin of one signal from another, when necessary. The direct (or practically direct) production of one signal from another is denoted by a hyphen (-), the indirect production through intermediate stages is denoted by (~), while the one characterized by both direct and indirect stages is denoted by ($\simeq$).

Thus, according to this terminology, SEG-FEO$\simeq$EP (read as "slow electrons from gas, directly caused by fast electrons from object, directly and indirectly caused by electrons from probe") are the slow (i.e. the conventional secondary) electrons produced from the gas by the ionizing action of the fast (i.e. conventional backscattered) electrons from object, caused by the unscattered electron probe. Similarly, CE$\simeq$FEO$\simeq$EP are the avalanche gaseous electrons connected to the useful (i.e. image producing) fast electrons from the object; the FEO first produce SEG, which, in turn, start electron avalanches in the presence of a strong electric field; the resulting CE may have a broad distribution of energies outside the 50 eV limit. The CE$\simeq$EP' (reading "cascade electrons directly and indirectly caused by scattered electrons from probe") are ionization electrons contributing only to the background noise of the image.

This is only a brief note on the new terminology, essential for this paper, and a more detailed justification of it can be found in the paper introducing it (Danilatos, 1990b); the reader would be helped by referring to it.

Electron Probe

For comparison purposes, we may describe the electron probe current density distribution with a Gaussian distribution function. As the beam propagates through the gas, it can be assumed that electrons are removed uniformly from it and the distribution retains its form. The intensity of the beam is decreased exponentially by a factor exp(-m), where m is the average number of electron collisions with the gas per incident electron, and, hence, the probe distribution is

$$j(r) = \frac{I_b}{2\pi c^2}\exp\left(\frac{r^2}{2c^2} - m\right) \quad \cdots EP \qquad (1)$$

where I_b is the incident electron beam current prior to its entry in the gas and c the standard deviation.

The current I(r) contained within a disk of

radius r is

$$I(r) = \int_0^r j(r')2\pi r'dr' \qquad (2)$$

$$\therefore \quad I(r) = I_b \exp(-m)\left[1-\exp\left(\frac{r^2}{2c^2}\right)\right] \quad \cdots EP \qquad (3)$$

Electron Skirt

The electrons removed from the original beam propagating through the gas form a kind of a "skirt" around the probe (Danilatos, 1988). It is of fundamental importance to determine the electron density distribution in the skirt, as this might have a decisive effect on the probe profile and, hence, on the contrast and resolution of the instrument. The electron scattering by gas in the scanning electron microscope has been examined theoretically for the case of single scattering (Moncrieff et al., 1979). However, the conclusions from that examination were restricted to apply only to the outer regions of the electron skirt, whereas it was further reported by Moncrieff et al. (1979) that the useful probe doubled its original diameter, as the pressure was raised; this was observed experimentally by scanning the beam across a sharp edge. The difference between theoretically derived and experimentally measured profiles was attributed to the fact that only single scattering was considered. To clarify this outstanding question, a rigorous theoretical and experimental survey was undertaken by Danilatos (1988), who considered the case of plural scattering. The conclusion of this survey was that the density of the skirt was orders of magnitude weaker than the unscattered fraction remaining in the original spot, throughout the entire range of the skirt, i.e. including the immediate vicinity of the useful probe spot. This conclusion was confirmed by careful experimental measurements, and the experimental observations by Moncrieff et al. were questioned.

The analytical method used for plural scattering is quite complex to apply and it was restricted only to monatomic gases, namely to argon. Its application to molecular gases is further complicated by the complex expressions of the differential cross-sections required. As the main conclusions arrived at from the study of electron skirts in argon are believed to be valid also in other gases, we only need estimates of the widths of the skirts in different gases for the purpose of finding the relative importance of these widths to the distributions of charge from the various signals from the specimen. To easily achieve this, below, we re-consider the use of analytical expressions from single scattering theory, which is much simpler for routine calculations with molecular gases, such as nitrogen, usually found in the ESEM.

First, a comparison of the results from plural scattering with those from single scattering theory is made. It can be easily shown (Moncrieff et al., 1979; Danilatos, 1988) that the probability $V(r)2\pi r\delta r$ to find an electron scattered within an elementary annulus $2\pi r\delta r$ is

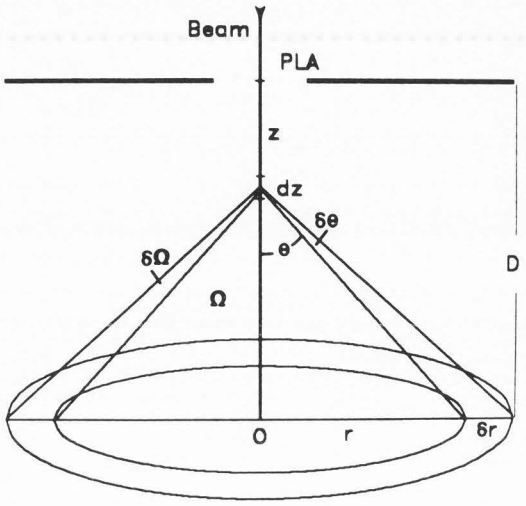

Fig. 1 An electron in the beam passing the pressure limiting aperture PLA undergoes a collision between z and z+dz and is scattered through an angle θ in the interval $\delta\theta$ (i.e. in the solid angle $\delta\Omega$) to finally strike a plane between r and r+δr.

$$V(r)2\pi r\delta r = \int_0^D \exp(-\sigma_T nz)\frac{d\sigma}{d\Omega}\delta\Omega n dz \qquad (4)$$

where n is density of gas particles, σ_T the total scattering cross-section of the gas and the other geometrical parameters are explained in Fig. 1. From this figure we also find that

$$\delta r = \frac{r\delta\theta}{\sin\theta\cos\theta} \quad \text{and} \quad \delta\Omega = 2\pi\sin\theta\delta\theta \qquad (5)$$

The average number m of collisions per electron is given by

$$m = \sigma_T nD = \frac{\sigma_T pD}{kT} \qquad (6)$$

and, thus, the electron density at a distance r from the axis is

$$j(r) = \frac{mI_b}{\sigma_T Dr^2}\int_0^D \exp\left(\frac{m}{D}z\right)\frac{d\sigma}{d\Omega}\sin^2\theta\cos\theta dz \quad \cdots EP' \qquad (7)$$

where the differential cross-section $d\sigma/d\Omega$ is usually expressed as a function of angle θ, which in terms of z is

$$\theta = \tan^{-1}\left(\frac{r}{D-z}\right) \qquad (8)$$

An analytical derivation of the differential cross-section has been presented by Lenz (1954) and adapted by Jost and Kessler (1963) and Danilatos (1988). The differential cross-section is the sum

of an elastic and an inelastic term. For atoms, the elastic term is

$$\frac{d\sigma_e}{d\Omega} = \frac{AZ}{16\left[\sin^2(\theta/2)+\sin^2(\theta_0/2)\right]^2} = |f(\theta)|^2 \quad (9)$$

and the inelastic term

$$\frac{d\sigma_i}{d\Omega} = \frac{A(\theta^2+\theta_E^2+2\theta_0^2)}{(\theta^2+\theta_E^2)(\theta^2+\theta_E^2+\theta_0^2)^2} \quad (10)$$

where

$$\theta_0 = \lambda/2\pi\mathbb{R} \quad (11)$$

$$\theta_E = J/4E \quad (12)$$

and

$$A = \frac{\lambda^4 Z(1+E/511000)^2}{4\pi^4 a_H^2} \quad (13)$$

with λ the electron wavelength given by

$$\lambda = 1.226\times10^{-9}(E+9.778\times10^{-7}E^2)^{-1/2} \quad (14)$$

and E the electron beam accelerating voltage in eV, J the ionization energy of the gas in eV, $\mathbb{R}$ the atom radius and a_H the Bohr radius. The atom radius may be derived from (Burge and Smith, 1962)

$$\mathbb{R} = \left[f_e(0)\frac{a_H}{2Z}\right]^{1/2} \quad (15)$$

where $f_e(0)$ is the scattering amplitude for electrons.

For molecules, the elastic differential cross-section is (Massey, 1969)

$$\frac{d\sigma_e}{d\Omega} = \sum_n \sum_m f_n(\theta) f_m(\theta) \frac{\sin(qr_{nm})}{qr_{nm}} \quad \text{(molecules)} \quad (16)$$

where $q=4\pi\sin(\theta/2)/\lambda$, r_{nm} is the inter-atomic distance between atoms n and m and $f_n(\theta)$ is the scattering amplitude for the n^{th} atom, and is given by Eq. (9). The corresponding inelastic term may be taken, as a good approximation, equal to the sum of all atomic differential cross-sections in the molecule

$$\frac{d\sigma_i}{d\Omega} = \sum_j \frac{d\sigma_{ij}}{d\Omega} \quad \text{(molecules)} \quad (17)$$

The accuracy and conditions, under which the above formulae are valid, have been summarized together with a tabulation of various constants for a selection of gases elsewhere (Danilatos, 1988). From the differential cross sections, the total cross-sections can be easily found.

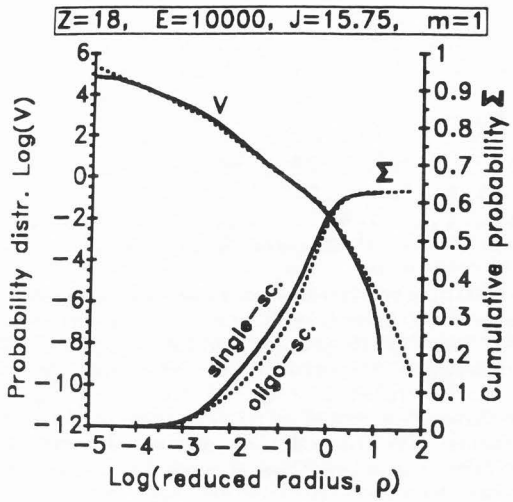

Fig. 2 Probability (V) and cumulative probability (Σ) distribution functions versus reduced radius in the single scattering and in the oligo-scattering regimes.

From Eq. (7) we obtain for the total current within a disk of radius r

$$I(r) = \int_0^r j(r')2\pi r'dr' \quad \cdots EP' \quad (18)$$

It can be shown, as is actually expected, that in the oligo-scattering regime, where m<3,

$$I(r) = \int_0^\infty j(r')2\pi r'dr' = I_b(1-e^{-m}) \quad \cdots EP' \quad (19)$$

The term e^{-m} is the fraction of electron beam that survives without scattering.

In order to compare results from previous work using plural scattering theory, the curves of probability distribution (i.e. $j(r)/I_b$) and cumulative probability (i.e. $\Sigma=I(r)/I_b$) have been redrawn from Danilatos (1988) in Fig. 2 together with new ones calculated from Eqs. (7) and (18) above. The case is for argon with E=10000 eV, J=15.75 eV and m=1. In this figure, the curves have been plotted versus a reduced radial distance ρ that relates to the real radial distance r as

$$\rho = \frac{2\pi\mathbb{R}r}{\lambda D} \quad (20)$$

The various equations depend only on the ratio r/D and only weakly on the electron beam energy, if expressed in terms of this reduced radius (Jost and Kessler, 1963). Close examination of the two sets of curves shows that electrons are removed from areas of medium radial distances, as we go from single scattering to plural scattering; that is, there are more electrons close to the axis and in the outer regions of the skirt as m increases. The difference is more pronounced with the cumulative probabilities. It is interesting to note

that the latter difference decreases towards the outer region, so that if we were interested in the overall width of the skirt, the single scattering theory would produce a close result. However, if we were to consider widths at half of the total scattered current (i.e. at $I(\infty)/2$), then the two methods may yield significant differences, depending on the value of m. Generally, the two methods produce similar results that approach each other as $m \to 0$.

It should be pointed out that the distributions in Fig. 2 are for an infinitely thin electron beam, or for sufficient distance away from a finite width beam. They only represent the scattered fraction of electrons and, hence, the cumulative probability reaches only the value of 0.63, of which the difference from unity is simply the unscattered fraction (e^{-1}) remaining on the axis of the system. To see the effect on the profile of a finite beam in the immediate neighborhood of the beam, one must combine the distribution of Eq. (7) with that of the beam given by Eq. (1). This has been done for plural scattering and found that the intensity of the scattered fraction is about two orders of magnitude less than the intensity of the unscattered fraction with a beam having c=0.0001 reduced units at m=1 (see Danilatos, 1988). Therefore, the single scattering theory would produce an even greater difference, as the distribution curve lies lower at short distances (see Fig. 2). The relative difference of intensity between the probe and skirt in the immediate vicinity of the probe is greater the smaller the probe diameter. In conclusion, both theories as well as experiment agree that the unscattered fraction from the original spot can be separated out from the broad and weak skirt; in addition, we may use the single scattering equations to make estimates of the overall width and behavior of the skirt towards its outer regions.

Profiles for molecular nitrogen have been computed at 10 keV by use of Eqs. (7) and (18), from which the reduced radius with 50% and 90% of the total skirt current have been calculated in the range $0<m<3$; the limit $m=3$ corresponds to 95% of the beam being scattered. In both cases, the widths increase little versus m, as follows:

$$\rho(50\%) = 0.052+0.013m \qquad (21)$$

$$\rho(90\%) = 0.61+0.09m \qquad (22)$$

By combining Eqs. (6), (14), (20), (21) and (22) and substituting various constants (T=293 K), we find the dependency of width in practical terms as

$$r(50\%) = \frac{0.354D+2.174\times10^{19}\sigma_T pD}{(E+9.778\times10^{-7}E^2)^{1/2}} \qquad pD<2 \qquad (23)$$

$$r(90\%) = \frac{4.128D+1.503\times10^{20}\sigma_T pD}{(E+9.778\times10^{-7}E^2)^{1/2}} \qquad pD<2 \qquad (24)$$

The above equations are valid in SI units except E that is expressed in eV; The electron beam energy was not replaced with E=10000 eV, as it should, but rather left as a parameter to be varied around

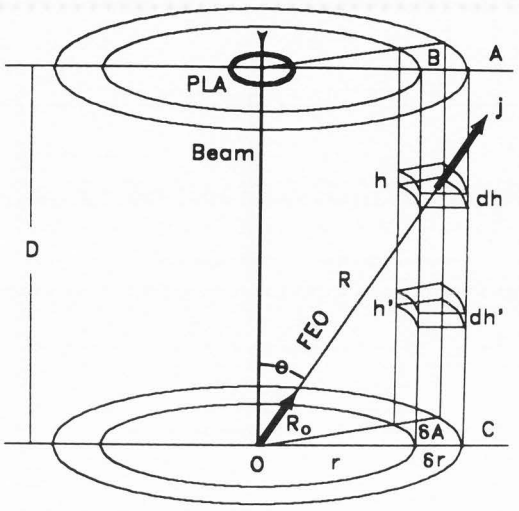

Fig. 3 The FEO originating from O have a current density j in the neighborhood of point (R,θ), or (R,h), and the ionization charge produced in the volume element $\delta A dh$ flows between the anode (A) and cathode (C) in the elementary column at B.

this value. This is allowed as an approximation, because Eqs. (21) and (22) depend weakly on accelerating voltage. The total cross-section strongly depends on the beam energy; at E=10000 eV, $\sigma_T=5.7\times10^{-21}$ m^2. The equations presented are all approximations giving good estimates, but, eventually experimental measurements should be used to determine precise values once and for all. The theoretical considerations presented can form a basis, and the ESEM provides a new precision instrument for measurements in particle impact phenomena.

Fast Electrons From Object

The FEO are distributed both over energy and solid angle as they emerge from the beam-specimen interaction. This property is formally expressed by the derivative of the FEO coefficient η with respect to energy E and solid angle Ω as $d\eta^2/dEd\Omega$, which is a characteristic function of the specimen. We can initially consider the distribution of FEO only over solid angle, irrespective of energy. Such a distribution depends both on the material and, mainly, on the topography of the specimen, i.e. on the angle of incidence of the beam on the specimen surface. Two cases of distribution are considered in this work: First, the well known *cosine* distribution, which describes normal beam incidence (see, for example, Reimer, 1985), is used as a basis to determine all relevant ionization currents. However, the same details of derivation are applicable with any other distribution. Thus, because the cosine distribution describes a *well polished* surface, the *uniform* distribution being a more "realistic" ave-

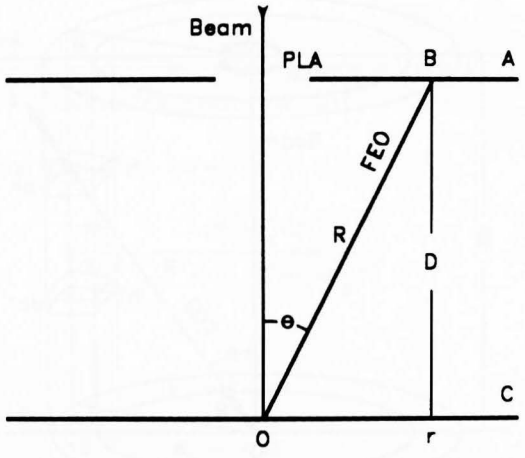

Fig. 4 Schematic defining the parameters for FEO current received by electrode A.

rage case is also considered towards the end of this paper, without repeating the same steps of derivations. For the cosine function we have:

$$\frac{d\eta}{d\Omega} = \frac{\eta_t \cos\theta}{\pi} \qquad (25)$$

where θ is the scattering angle from the normal of the specimen surface and η_t the total FEO coefficient. From this, we can easily derive the current density j due to FEO at a point with polar coordinates (R,θ) from the point of beam incidence (see Fig. 3). This is found to be:

$$\vec{j}(R,\theta) = \frac{\eta_t I_b \cos\theta}{\pi R^2}\,\vec{R}_0 \quad \cdots\text{FEO} \qquad (26)$$

where the current density is designated as a vector along the direction of the unit position vector $\vec{R}_0$. Here, we consider both FEO≈EP and FEO≈EP'. The FEO due to the electron beam skirt emerge from an area of the order of tens of microns, which is several orders of magnitude smaller than the size of the electrodes, or the region in the gas, over which they normally travel; hence, initially, they may all be considered as coming from a point source.

The current density due to FEO at point B on the top plane electrode A (see Fig. 4), i.e. the current per unit area of *electrode*, at a radial distance r from the optical axis and a vertical distance D from the specimen is

$$j(r,D) = \frac{\eta_t I_b D^2}{\pi(D^2+r^2)^2} \equiv \frac{\eta_t I_b}{\pi D^2 Q^4} \quad \cdots\text{FEO} \qquad (27)$$

where

$$Q = \left(1 + \frac{r^2}{D^2}\right)^{1/2} \qquad (27')$$

In the above, the relations $r=R\sin\theta$ and $D=R\cos\theta$ were used, while the factor Q is introduced to simplify the many expressions, in which it is frequently encountered. As both Eqs. (26) and (27) describe current densities at a point, the letter j has been used in both cases for simplicity; the accompanying spherical coordinates will signify that we describe the density in space, whereas the cylindrical ones refer to a horizontal plane (here, the electrode).

By integrating $j(r)2\pi r dr$ between 0 and r we find the current collected by a disk electrode:

$$I(r,D) = \eta_t I_b\left[1 - \frac{1}{Q^2}\right] \quad \cdots\text{FEO} \qquad (28)$$

For a given annular collector with fixed radii r_1 and r_2 there is a maximum current I_{max} at a distance D_{max}:

$$I = \eta_t I_b \frac{r_2 - r_1}{r_1 + r_2} \quad \text{at} \quad D_{max} = \sqrt{r_1 r_2} \qquad (29)$$

FEO in Gas, Low Field

The equations developed above are applicable to FEO both in vacuum and gaseous conditions, provided that, in the latter case, the number of scattering events per FEO is kept low, so that the total deflection of electrons is small compared to the size of detection electrode and the distance traveled by them. In a gas, a certain proportion of collisions results in ionizations. The function of primary ionization rate $N(R,\theta)$, i.e the number of ionizations per unit volume per unit time at point (R,θ) in the gas, arising from the direct action of the FEO, relates to the pressure p and to the ionization efficiency S (i.e. number of ionizations per unit pressure per unit length), as:

$$N(R,\theta) = \frac{j(R,\theta)pS}{e} \quad \cdots(S\&F)\text{-FEO} \qquad (30)$$

where e is the electron charge. The *ionization efficiency* S is a reduced factor to be distinguished from the *ionization efficiency coefficient* s (i.e. number of ionizations per unit length) and to which relates by S=s/p. The FEG are the fast electrons from gas, known as δ-rays (e.g. Corson and Wilson, 1948), but they constitute a small fraction of all the electrons produced from gas, which are usually SEG.

The charge (positive or negative) generated at a point in the gas per unit volume per unit time is, therefore,

$$eN = \frac{\eta_t I_b pS\cos\theta}{\pi R^2} = \frac{\eta_t I_b phS}{\pi(r^2+h^2)^{3/2}} \qquad (31)$$

Let us consider the case of a uniform electric field between two plane electrodes where the charge carriers, i.e. positive ions and electrons, drift in opposite directions towards the electrodes. Due to thermal agitation, the charges

also diffuse outwards at a certain rate depending on the intensity of the field, the gas pressure and the nature of gas. This effect is orders of magnitude less pronounced for the positive ions, because their temperature does not significantly exceed that of the neutral gas, whereas the electrons are much less thermally coupled with the gas and, as a result, their temperature significantly rises, as they gain energy from the external field. We may further restrict the case under consideration, where the conditions of field, gas, pressure and distance D are such that the magnitude of the outward diffusion is within fraction of a mm, whereas the electrodes extend over several mm or more; also, here, the field is low and does not trigger any avalanches from the ionization electrons produced by FEO, but is strong enough to result in complete collection of all electrons and ions generated by the FEO (condition of saturation ionization current). The extent of radial diffusion of electrons is considered later in this paper and a review of related theories has been presented by Danilatos (1990b).

Total ionization current

Under these conditions, we can calculate the ionization current density arriving at the top (or bottom) electrode. First, we consider the *total* current induced by both electrons and ions in the gas. This is done by integrating the current generated in an elementary column between the two electrodes at point B (see Fig. 3):

$$j(r,D) = \int_0^D eNdh = \frac{\eta_t I_b pS}{\pi}\int_0^D \frac{hdh}{(r^2+h^2)^{3/2}} \qquad (32)$$

$$\therefore\ j(r,D) = \frac{\eta_t I_b pS}{\pi}\left[\frac{1}{r} - \frac{1}{DQ}\right] \quad \cdots \text{S(E\&I)G-FEO} \qquad (33)$$

Here, the electrons and ions from the gas directly produced by the FEO are regarded as simply drifting in the gas without multiplication.

The corresponding *total* current within a disk of radius r is given by

$$I(r,D) = 2\eta_t I_b pDS\left(1 + \frac{r}{D} - Q\right) \quad \cdots \text{S(E\&I)G-FEO} \qquad (34)$$

Negative (or electron) ionization current

The derivations of ionization currents above were based on the simple method of counting the total number of electrons arriving at the top electrode, which is equal to the total number of positive ions arriving at the bottom electrode. As has been discussed elsewhere (Danilatos, 1990b; 1990c), the signal detected at each electrode is actually generated by induction only during the motion of charges between electrodes, whereas the current in the external circuit, due to a charged particle, ceases to flow, when the particle arrives at the respective electrode. The total signal induced on either electrode is due to both ions and electrons. When an electron/ion pair is formed at some point h from the bottom electrode (see Fig. 3), the electron travels a distance D-h to one electrode and the ion a distance h to the other electrode. In a uniform electric field, the electron is responsible for a fraction (D-h)/D and the ion for a fraction h/D of the total pulse induced; the total charge that flows in the external circuit is e. Because the electrons and the ions have different mobilities in the gas, which differ typically by three orders of magnitude, it may be necessary to consider the respective signals induced separately. For example, the time of flight of a particular charge between electrodes determines the frequency response of the system, and we need to know the relative magnitude of the electron and ion contributions. The simple counting method fails to supply the correct answers. Therefore, we resort to first principles of the theory of electricity as follows:

Two basic equations are used. The first:

$$I = q\upsilon/D \qquad (35)$$

relates the induced current I by the moving charge q with velocity υ between electrodes at distance D, and the second:

$$j = \rho\upsilon \qquad (36)$$

relates the velocity with the current density at a point and with the charge density ρ at the point.

Thus, in the column element with base δA and height dh at point h (see Fig. 3) the negative charge is $\rho_n(h)dh\delta A$, which, moving with drift velocity υ_n, induces a current $d\delta I$ in the external circuit

$$d\delta I = \frac{\upsilon_n \rho_n(h)dh\delta A}{D} \qquad (37)$$

The electron charge density at a point h is found by adding all the contributions of electrons generated in the column at points h' with h'<h. The rate of charge production in the volume element $dh'\delta A$ is $eN(h')dh'\delta A$ and, by the continuity principle, this charge crosses the area at point h at the same rate

$$dj(h)\delta A = eN(h')dh'\delta A \qquad (38)$$

Combining Eqs. (36) and (38) we find

$$\rho_n(h) = \frac{1}{\upsilon_n}\int_0^h eN(h')dh' \qquad (39)$$

$$\therefore\ \rho_n(h,r) = \frac{\eta_t I_b pS}{\pi\upsilon_n}\left[\frac{1}{r} - \frac{1}{(h^2+r^2)^{1/2}}\right] \qquad (40)$$

Hence, Eq. (37) becomes

$$d\delta I = \frac{dh\delta A}{D}\int_0^h eN(h')dh' \qquad (41)$$

By integrating Eq. (41) with respect to h from 0 to D, we find the total current induced at the electrode by the charge in the elementary column. Because this current is collected by an area δA, the current density at the electrode is $j(r,D)=\delta I/\delta A$:

$$j(r,D) = \int_0^D \frac{dh}{D} \int_0^h eN(h')dh' \qquad \cdots SEG\text{-}FEO \quad (42)$$

After integrating we find

$$j(r,D) = \frac{\eta_t I_b pS}{\pi}\left[\frac{1}{r} + \frac{1}{D}\ln\frac{r}{D(1+Q)}\right] \qquad \cdots SEG\text{-}FEO \quad (43)$$

The corresponding disk current is found to be

$$I(r,D) = \eta_t I_b pDS\left(1 - Q + 2\frac{r}{D} + (\frac{r}{D})^2\ln\frac{r}{D(1+Q)}\right)$$

$$\cdots SEG\text{-}FEO \quad (44)$$

For later derivations, it is instructive to note that we can arrive at the same result as Eq. (42) as follows:

The column element $dh\delta A$ at h produces a current $eN(h)dh\delta A$ that is constant in the column for $h'>h$. This current corresponds to a constant charge density $d\rho_n = dj(h')/\upsilon_n$ for $h'>h$, which is

$$d\rho_n = \frac{eN(h)dh}{\upsilon_n}$$

Due to this partial density, a partial current $d^2\delta I$ is induced

$$d^2\delta I = \frac{d\rho_n\, dh'\delta A\, \upsilon_n}{D} = \frac{eN(h)dhdh'\delta A}{D}$$

$$\therefore \quad d\delta I = \int_h^D d^2\delta I = eN(h)dh\delta A\left(1 - \frac{h}{D}\right)$$

$$\therefore \quad j(r,D) = \frac{\delta I}{\delta A} = \int_0^D eN(r,h)\left(1 - \frac{h}{D}\right)dh \qquad (45)$$

which, after integration, yields the same result as Eq. (43).

Positive ionization current

Along the same lines, we can derive the corresponding equations for the positive ion density and current. Taking care of the limits of integrations and replacing the electron drift velocity with the ion drift velocity υ_p, we find

$$\rho_p(h) = \frac{1}{\upsilon_p}\int_h^D eN(h')dh' \qquad (46)$$

$$\therefore \quad \rho_p(h,r) = \frac{\eta_t I_b pS}{\pi\upsilon_p}\left[\frac{1}{(r^2+h^2)^{1/2}} - \frac{1}{DQ}\right] \qquad (46')$$

The current induced is given by corresponding equations

$$j(r,D) = \int_0^D \frac{dh}{D} \int_h^D eN(r,h')dh' \equiv \int_0^D eN(r,h)\frac{h}{D}\,dh$$

$$\cdots SIG\text{-}FEO \quad (47)$$

which, after integration, yields

$$j(r,D) = \frac{\eta_t I_b pS}{\pi}\left[\frac{1}{D}\ln\frac{r}{D(1+Q)} - \frac{1}{DQ}\right] \qquad \cdots SIG\text{-}FEO \quad (48)$$

Similarly, by integration, the corresponding disk current is found to be

$$I(r,D) = \eta_t I_b pDS\left(1 - Q - (\frac{r}{D})^2\ln\frac{r}{D(1+Q)}\right)$$

$$\cdots SIG\text{-}FEO \quad (49)$$

The positive ions move in the opposite direction to that of electrons and, because they also have opposite charge, they induce a current in the same direction as that by the electrons. We can confirm that by summing Eqs. (43) and (48) we find the same total current as that given by Eq. (33). Although one could derive the equations for positive ions by simply subtracting the ones for electrons from the total current, the derivation and result are presented above both for theoretical completeness and for easy engineering reference.

The total space charge density is found by algebraically summing Eqs. (40) and (46'):

$$\rho(r,h) = \frac{\eta_t I_b pS}{\pi}\left[\left(\frac{1}{\upsilon_p} + \frac{1}{\upsilon_n}\right)\frac{1}{(h^2+r^2)^{1/2}} - \frac{1}{\upsilon_p DQ} - \frac{1}{\upsilon_n r}\right]$$

(50)

SEO in Gas, Low Field

The slow electrons from object, in the presence of gas and low external uniform field, collide with the gas molecules without ionizing it and acquire a steady drift velocity in the direction of the field. Due to thermal agitation, they also diffuse radially, so that by the time they reach the upper electrode, a fraction of them is located within a disk of radius r. This fraction has been calculated by Huxley and Zaazou (1949) and their result is adapted as follows: If the slow electron yield coefficient is δ_t, then $\delta_t I_b$ current originates at the specimen surface, and the current I(r,D) reaching the anode within r is

$$I(r,D) = \delta_t I_b \frac{\delta_t I_b}{Q}\exp\left[\frac{eV}{2kT\varepsilon}(1-Q)\right] \qquad \cdots SEO \quad (51)$$

where V is the applied potential, k Boltzmann's constant, T absolute temperature and ε is the ratio of thermal energy of electrons to the thermal energy of the host gas molecules. Values of the latter factor have been compiled from the literature by Danilatos (1990b). The diameter within which the majority of electrons arrive at the top electrode can vary greatly, but, for most practical cases, it is of the order of mm. Thus, all the SEO due to both the useful probe and the skirt can be considered as originating from a small region, i.e. a point.

The corresponding current distribution can be found by a simple differentiation with respect to

r and then by division by $2\pi r$:

$$j(r,D) = \frac{\delta_t I_b}{2\pi D^2 Q^2}\left[\frac{eV}{2kT\varepsilon} + \frac{1}{Q}\right]\exp\left[\frac{eV}{2kT\varepsilon}(1-Q)\right]$$

$\cdots$SEO (52)

SEO in Gas, High Field

Total current

When the external field is sufficiently strong to impart enough energy to the drifting electrons to ionize the gas, it can be easily shown (see review by Danilatos, 1990b) that the total current I in the external circuit increases by a factor

$$\frac{I}{\delta_t I_b} = e^{\alpha D} \quad \cdots C(E\&I)\simeq SEO \tag{53}$$

where α is the first Townsend coefficient. This represents the total effect of both electrons and ions in the steady state condition, i.e when we allow enough time for the slower positive ions to reach the cathode. The avalanche of electrons reaching the top electrode has the same radial distribution as the SEO at low field, i.e. as given by Eqs.(51) and (52) according to Townsend and Tizard (1913). The positive ions do not spread by any appreciable amount any further as they move to the bottom electrode. Therefore, we only have to multiply these equations by the gain factor $e^{\alpha D}$. However, if we need to know the contribution of the electrons separately from that of the positive ions, we have to establish the corresponding gain factors as follows:

Electron current

In an analogous manner as previously, we need to define a linear charge density $\lambda_n(h)$

$$\lambda_n(h) = \frac{dq}{dh} \tag{54}$$

where dq is the electron charge in a slab of thickness dh at h (see Fig. 5). Because $dh=v_n dt$, we get for the electron current I_n crossing a plane at h

$$I_n(h) = v_n \lambda_n(h) \tag{55}$$

The increase of electrons in the slab is represented by

$$dI_n = \alpha I_n dh \tag{56}$$

from which the current of electrons at h is:

$$I_n(h) = \delta_t I_b e^{\alpha h} \tag{57}$$

and thus

$$\lambda_n(h) = \frac{\delta_t I_b}{v_n} e^{\alpha h} \tag{58}$$

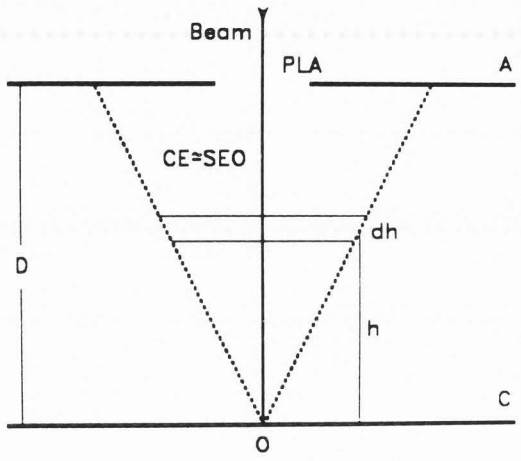

Fig. 5 The SEO originating from O multiply in an avalanche (dotted lines), as they drift towards A by the field and outwards by thermal agitation.

The induced current in the external circuit by the electrons in the slab is

$$dI = \frac{v_n \lambda_n(h) dh}{D} \tag{59}$$

By integrating Eq. (59) from O to D, we find the total current induced by the electrons alone, and the corresponding amplification factor:

$$\frac{I}{\delta_t I_b} = \frac{1}{\alpha D}\left(e^{\alpha D} - 1\right) \quad \cdots CE\simeq SEO \tag{60}$$

Positive ion current

The electrons create positive ions along their path to the anode, but the ions thus formed do not further ionize the gas as they drift towards the cathode. In addition, they do not diffuse outward in any significant amount, because their ε factor is close to unity for the fields frequently used in the ESEM. The linear density of positive ions $\lambda_p(h)$ again satisfies a relation

$$\lambda_p(h) = \frac{I_p}{v_p} \tag{61}$$

where I_p is the positive ion current flowing at h. This is due to all ions from h'>h, which are formed at the same rate as the corresponding electrons. For a slab dh' at h' this rate is simply given by Eq. (56) as

$$dI_p = dI_n = \alpha I_n dh' = \alpha \delta_t I_b e^{\alpha h'} dh' \tag{62}$$

from which

$$I_p = \int_h^D \alpha \delta_t I_b e^{\alpha h'} dh' = \delta_t I_b \left(e^{\alpha D} - e^{\alpha h}\right) \tag{63}$$

Substitution of this result in Eq. (61) leads to

$$\lambda_p(h) = \frac{\delta_t I_b}{v_p}\left(e^{\alpha D} - e^{\alpha h}\right) \qquad (64)$$

Finally, the current induced by the moving positive charge is found by integration as

$$I = \int_0^D dI = \int_0^D \frac{v_p \lambda_p(h) dh}{D}$$

$$\therefore \quad \frac{I}{\delta_t I_b} = e^{\alpha D}\,\frac{1}{\alpha D}\left(e^{\alpha D} - 1\right) \quad \text{CI}\simeq\text{SEO} \qquad (65)$$

which is the gain factor for the avalanche ions due to SEO. We can immediately confirm that, by adding the results of Eqs. (60) and (65), we produce the result of Eq. (53), as expected. It is worthwhile noting that the gain factor for electrons includes the contribution to it of the original electrons (i.e. SEO), which is equal to unity, whereas the factor for positive ions is entirely due to the ionization of the gas.

FEO in Gas, High Field

As we have seen, the FEO have enough energy of their own to create a primary, or initial, ionization in the gas, mainly the S(E&I)G-FEO. In the presence of a strong enough field, the SEG-FEO produce secondary, or additional, ionization as they drift towards the anode. Each SEG-FEO starts a new avalanche that spreads according to Eq. (51) with a gain similar to Eqs. (53), (60) and (65), but properly modified to take into account the variable position of the starting point (see Fig. 6). The general case is quite complex to express analytically, but for the present purposes, it would be sufficient to consider the simple case where the spread of the avalanches is confined within a small diameter column, in which we can integrate the total effect. Again we distinguish three cases:

Total current

In a similar fashion, the total current induced by the moving electrons and ions can be easily found by counting the number of electrons reaching the anode. This calculation yields the correct answer, if we wait enough time for the positive ions to complete the circuit. The element in the column of Fig. 6 produces an initial current $eN(r,h)dhdA$, which is then amplified by a factor $e^{\alpha(D-h)}$, so that the point current density is found by integrating over the height of the element

$$j(r) = \int_0^D eN(r,h)e^{\alpha(D-h)}dh \qquad (66)$$

$$\therefore j(r,D) = \frac{\eta_t I_b pS}{\pi}\int_0^D \frac{he^{\alpha(D-h)}dh}{(r^2+h^2)^{3/2}} \quad \cdots\text{C(E\&I)}\simeq\text{FEO} \qquad (67)$$

The total current collected by a disk of radius r is

$$I(r,D) = 2\eta_t I_b pS\int_0^D\left[1 - \frac{h}{(r^2+h^2)^{1/2}}\right]e^{\alpha(D-h)}dh$$

$$\cdots\text{C(E\&I)}\simeq\text{FEO} \qquad (68)$$

It is worthwhile noting that Eq. (68) is valid even if the spread of each individual avalanche is greater than the area δA of the elementary column, but much smaller than the area of the disk electrode. This is because $j(r,D)\delta A = \delta I$, where δI is the current *induced* in the *external* circuit by all the avalanches starting inside the elementary column, but may spread outside the boundaries of it, as it develops towards the anode.

Electron current

By following the same reasoning as in previous sections, we can derive the separate contributions to the induced current by the electrons and ions. Omitting the intermediate steps, but subject to the same conditions as in the previous section for the total current, we finally find

$$j(r,D) = \int_0^D eN(r,h)\frac{1}{\alpha D}\left(e^{\alpha(D-h)} - 1\right)dh \qquad (69)$$

$$\therefore\ j(r,D) = \frac{\eta_t I_b pS}{\pi\alpha D}\int_0^D \frac{h}{(r^2+h^2)^{3/2}}\left(e^{\alpha(D-h)} - 1\right)dh$$

$$\cdots\text{CE}\simeq\text{FEO} \qquad (70)$$

The disk current is

$$I(r,D) = \frac{2\eta_t I_b pS}{\alpha D}\int_0^D\left[1 - \frac{h}{(r^2+h^2)^{1/2}}\right]\left(e^{\alpha(D-h)} - 1\right)$$

$$\cdots\text{CE}\simeq\text{FEO} \qquad (71)$$

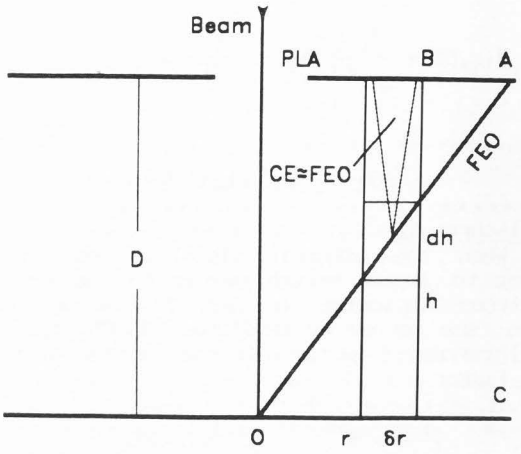

Fig. 6 Schematic of the parameters for the derivation of distribution equation for CE≃FEO. A FEO originating from O starts avalanches with the ionizing collisions along its track.

Positive ion current

The derivation of the equations for positive ions is a little more complicated, but it follows the same reasoning. Omitting the details here, the final equations are as follows.

The point current density is

$$j(r,D) = \int_0^D eN(r,h)\left[e^{\alpha(D-h)}\left(1-\frac{1}{\alpha D}\right)+\frac{1}{\alpha D}\right]dh \qquad (72)$$

$$\therefore\ j(r,D) = \frac{\eta_t I_b p S}{\pi\alpha D}\int_0^D \frac{h}{(r^2+h^2)^{3/2}}\left[e^{\alpha(D-h)}(\alpha D-1)+1\right]dh$$

$$\cdots \text{CI}\simeq\text{FEO} \qquad (73)$$

Finally, the disk current is

$$I(r,D)=\frac{2\eta_t I_b p S}{\alpha D}\int_0^D\left[1-\frac{h}{(r^2+h^2)^{1/2}}\right]\left[e^{\alpha(D-h)}(\alpha D-1)+1\right]dh$$

$$\text{CI}\simeq\text{FEO} \qquad (74)$$

The same condition applies for Eqs. (70) and (73), namely, that the avalanche widths are not appreciably greater than the width of the column of integration. However, Eqs. (71) and (74) are always valid, provided that the disk radius is much greater than the avalanche spread.

FEO in Gas with SEO-Retarding Field

All previous analysis was done with the field assumed to be in a direction that accelerates all electrons away from the specimen, i.e. from the bottom electrode towards the top electrode. If the electric field is reversed with sufficient intensity, then the SEO will be retarded back to specimen, leaving only the FEO as the active component for signal generation.

The S(E&I)G-FEO will simply move in opposite directions, and the Eqs. (32), (33) and (34) for the total ionization current are valid also for the present case, except that the current will flow in the opposite sense. However, the individual components for electrons and ions have different equations, when the polarity of the field is reversed: Because each of these species of charge carriers moves in an opposite direction, they simply exchange their travel paths and, because their equations depend on the travel paths in the uniform field, their corresponding equations should be simply exchanged; one can confirm this conclusion by following the same steps of derivation by use of the induction theory. Thus, the equation for electrons is

$$I(r,D) = \eta_t I_b p D S\left[1 - Q - \left(\frac{r}{D}\right)^2 \ln\frac{r}{D(1+Q)}\right]$$

$$\cdots \text{SEG-FEO} \qquad (75)$$

and for ions

$$I(r,D) = \eta_t I_b p D S\left[1 - Q + \frac{2r}{D} + \left(\frac{r}{D}\right)^2 \ln\frac{r}{D(1+Q)}\right]$$

$$\cdots \text{SIG-FEO} \qquad (76)$$

The situation for a high retarding field that causes avalanche amplification is, somehow, different. An analysis shows that the factor $e^{\alpha(D-h)}$ in the Eqs. (66)-(74) should be replaced with $e^{\alpha h}$. Therefore, for the total signal we have

$$j(r,D) = \frac{\eta_t I_b p S}{\pi}\int_0^D \frac{h e^{\alpha h} dh}{(r^2+h^2)^{3/2}} \qquad \cdots \text{C(E\&I)}\simeq\text{FEO} \qquad (77)$$

and

$$I(r,D) = 2\eta_t I_b p S\int_0^D\left[1-\frac{h}{(r^2+h^2)^{1/2}}\right]e^{\alpha h}dh$$

$$\cdots \text{C(E\&I)}\simeq\text{FEO} \qquad (78)$$

For the signal induced by electrons only we have

$$j(r,D) = \frac{\eta_t I_b p S}{\pi\alpha D}\int_0^D \frac{h}{(r^2+h^2)^{3/2}}\left(e^{\alpha h}-1\right)dh$$

$$\cdots \text{CE}\simeq\text{FEO} \qquad (79)$$

and

$$I(r,D) = \frac{2\eta_t I_b p S}{\alpha D}\int_0^D\left[1-\frac{h}{(r^2+h^2)^{1/2}}\right]\left(e^{\alpha h}-1\right)$$

$$\cdots \text{CE}\simeq\text{FEO} \qquad (80)$$

Finally, for the signal induced by ions only we have

$$j(r,D) = \frac{\eta_t I_b p S}{\pi\alpha D}\int_0^D \frac{h}{(r^2+h^2)^{3/2}}\left[e^{\alpha h}(\alpha D-1)+1\right]dh$$

$$\cdots \text{CI}\simeq\text{FEO} \qquad (81)$$

and

$$I(r,D)=\frac{2\eta_t I_b p S}{\alpha D}\int_0^D\left[1-\frac{h}{(r^2+h^2)^{1/2}}\right]\left[e^{\alpha h}(\alpha D-1)+1\right]dh$$

$$\cdots \text{CI}\simeq\text{FEO} \qquad (82)$$

Ionization from Electron Beam

The electrons from probe and from skirt produce ionization before the beam strikes the specimen and hence the produced current contributes only to the background noise. The ionization is confined within a relatively small radius and the corresponding distributions will not be derived here. For the present purposes, it will be sufficient to simply find the combined ionization current produced by the electron probe and the skirt

together, at low and high field.

It can be easily found that, at low field, the total ionization current is

$$I = I_b pSD \quad \cdots S(E\&I)G\text{-}E(P\&P') \tag{83}$$

The ionization current due to electrons only is

$$I = \tfrac{1}{2} I_b pSD \quad \cdots SEG\text{-}E(P\&P') \tag{84}$$

The ionization current due to ions only is, therefore, the same as in Eq. (84).

At high field, the total ionization current is

$$I = \frac{I_b pS}{\alpha}\left(e^{\alpha D}-1\right) \quad \cdots C(E\&I)\simeq E(P\&P') \tag{85}$$

The corresponding current induced by electrons only is

$$I = \frac{I_b pS}{\alpha}\left[\frac{1}{\alpha D}\left(e^{\alpha D}-1\right) - 1\right] \quad \cdots CE\simeq E(P\&P') \tag{86}$$

Finally, the corresponding current induced by ions only is

$$I = \frac{I_b pS}{\alpha}\left[\left(1-\frac{1}{\alpha D}\right)e^{\alpha D} + \frac{1}{\alpha D}\right] \quad \cdots CI\simeq E(P\&P') \tag{87}$$

Ionization Efficiency

Crucial to most of the derivations above is their dependence on the ionization efficiency S, which strongly depends on the electron energy and the nature of gas. This coefficient, or related ones, can be found in the literature. On many occasions, information is given on the ionization mean free path L_i, or on the ionization cross-section σ_i, which inter-relate as

$$L_i = \frac{1}{pS} = \frac{kT}{\sigma_i p} \tag{88}$$

In order to understand the relative magnitudes of the charge distributions in the ESEM, we consider a typical case, namely, the use of nitrogen as the filling gas. For this, data on the ionization efficiency have been taken from Engel (1965) and Massey (1969) and fitted with empirical equations in two ranges of energy as follows:

$$S(E) = 485.63E^{1.3}\exp(-7.05E^{0.7}) \quad \text{for } 0.02<E<0.3 \tag{89}$$

and

$$S(E) = AE^{-B} \equiv 1.733E^{-0.862} \quad \text{for } 0.3<E<30 \tag{90}$$

where the energy is expressed in keV and all other quantities in SI units. As there is some variation in the data published by various authors, the above formulae provide satisfactory means for engineering considerations.

The distribution of FEO over energy depends mainly on the target material and is almost independent of the incident beam energy, provided that the distribution is plotted as a reduced energy $W=E/E_b$, where E is the FEO energy and E_b the beam energy (Matsukawa et al., 1974). Let us consider normal beam incidence on a copper specimen with a flat surface. For this case, the experimental results by Matsukawa et al. have been fitted with the empirical equation

$$\frac{d\eta}{dW} = \sum_{i=0}^{5}(-1)^i A_i W^i \equiv$$

$$\equiv 0.05-0.23W+2.25W^2-7.408W^3+15.784W^4-10.29W^5 \tag{91}$$

This equation does not include the fine structure (peaks) of the Auger electrons, or the low-loss peak of the FEO, but it closely represents about 90% of the FEO. The error will be small, if Eqs. (89), (90) and (91) are used to find a practical mean for the ionization efficiency as:

$$\langle S\rangle = \frac{\int_{E_{min}}^{E_b} S(E)\frac{d\eta}{dE}dE}{\int_{E_{min}}^{E_b}\frac{d\eta}{dE}dE} \tag{92}$$

The main question here is with regard to the lower limit of integration E_{min}. As was pointed out earlier, the distribution of ionization in the bulk of the gas caused by FEO can be expressed by the equations arrived at, provided that (a) the FEO have high enough energy and (b) undergo a relatively small number of collisions, so that they do not lose significant energy and they are not deflected significantly in the gas region under consideration. Clearly, the equations are not valid for relatively high (travel distance)×(pressure) conditions and for the low energy FEO, cases which need to be treated separately. However, for a great many conditions of design and applications of ESEM, we may proceed with our derivations. The lower limit E_{min} must be much higher than the energy loss of a FEO between two consecutive ionizing collisions. For nitrogen, this energy loss (in the form of ionization, excitation etc.) has a relatively constant mean of 34.6 eV for E>2 keV, but varies at lower energy (see literature surveys by Danilatos, 1988; 1990b). For example, an electron of 0.4 keV produces an average of 4 ionizations, but at 0.8 keV it produces 13 ionizations, because a sharp increase occurs from 0.7 keV (Cobine, 1941). Therefore, E_{min}=0.8 keV seems a reasonable choice. This choice also satisfies a limitation imposed by the external potential between electrodes. Potentials up to 400 V have been used, and, therefore, the trajectories of FEO with energies of the same order (i.e. 400 eV) or lower will be affected.

For E>0.8 keV we can use the simple Eq. (90) in Eq. (92) to arrive at the analytical

expression:

$$\langle S\rangle = \frac{\sum_{i=0}^{5}(-1)^i \frac{A_i}{i-B+1}\left(1-W_{min}^{i-B+1}\right)}{\sum_{i=0}^{5}(-1)^i \frac{A_i}{i+1}\left(1-W_{min}^{i+1}\right)} AE_b^{-B} \equiv CS(E_b) \quad (93)$$

where the constant C can be readily calculated. The significance of E_{min} in our calculations depends on the value of E_b through $W_{min}=E_{min}/E_b$. Thus, taking $\eta_t=0.31$ for copper, we find that, for $E_b=1$, only 31.6% of FEO contribute to the calculation of <S>, and C=1.11. For $E_b=2$ we have 79.7% of FEO contributing and C=1.34, for $E_b=5$ we have 86.2% and C=1.47, for $E_b=10$ we have 87.4% and C=1.53 and for $E_b=30$ we have 88.2% and C=1.64. Therefore, for $E_b>2$ keV practically all the FEO that are accounted for by the Matsukawa et al. distribution are included in the calculation of the <S>. For $E_b<2$ the fraction of FEO electrons with $E<E_{min}$ becomes significant.

The Gain Factor

Another critical parameter in the equations derived is the α-coefficient (first Townsend coefficient), which depends on the field, pressure and nature of gas. A literature survey on derivations for this coefficient together with tables of constants for various gases are presented elsewhere (Danilatos, 1988). A simple expression is

$$\alpha = Ap\exp\left(-\frac{B}{\mathscr{E}/p}\right) \quad (94)$$

where $\mathscr{E}$ is the intensity of the electric field and A and B are constants of the gas; for nitrogen A=9 1/Pam and B=256.5 V/Pam in the range $75<\mathscr{E}/p<450$.

Only the simple case of amplification factor $\exp(-\alpha D)$ is considered here, because, under the stable conditions sought, this describes quite adequately the gaseous gain. As the γ-processes start appearing, a higher gain is achieved, but the situation becomes quickly unstable. The γ-processes are various mechanisms whereby new electrons are ejected from the cathode resulting in new generations of electron avalanches in the gas. These mechanisms operate singly or simultaneously and are responsible for the ultimate breakdown of the discharge as we increase the applied bias. This regime ought to be avoided, and maximum amplification is preferred through the gaseous amplification alone (i.e. through the α-process). This situation has been discussed in detail together with an extended literature survey elsewhere (Danilatos, 1990b).

A small correction to the gain factor may be more pertinent to briefly consider here, especially for the lower range of electrode bias. For a given field, there is a minimum electrode separation, below which no gain can be achieved, because the electron does not gain enough energy to ionize the gas (see e.g. Weston, 1968). This minimum distance D_m corresponds to the minimum effective ionizing potential of the gas V_m through the equation

$$\frac{V_m}{D_m} = \frac{V}{D} = \mathscr{E} \quad (95)$$

and, thus, the actual gain factor G is

$$G = \exp\left(\alpha(D-D_m)\right) = \exp(f\alpha D) \quad (96)$$

where the correction factor f is

$$f = 1 - \frac{V_m}{V} \quad (97)$$

This becomes more significant at low voltage, especially with the equation for SEO. This correction may be incorporated in all the relevant equations, but its effect is found to be much smaller than the uncertainties caused by other effects, such as, for example, the purity of the gas used. This correction is not important for the main features of the distribution functions derived above.

Examples of Distribution

Let us apply some of the equations to a typical case, for which we choose the following parameters. We use a 10 keV electron beam, for which we can calculate <S>=0.38 from Eq. (93). The electron beam is described by a Gaussian distribution given by Eqs. (1) and (3) with $c=10^{-8}$ m. We may also choose a pressure of p=1000 Pa and distance D=0.001 m. The parameter ε for nitrogen in Eq. (51) presents the difficulty that it has been

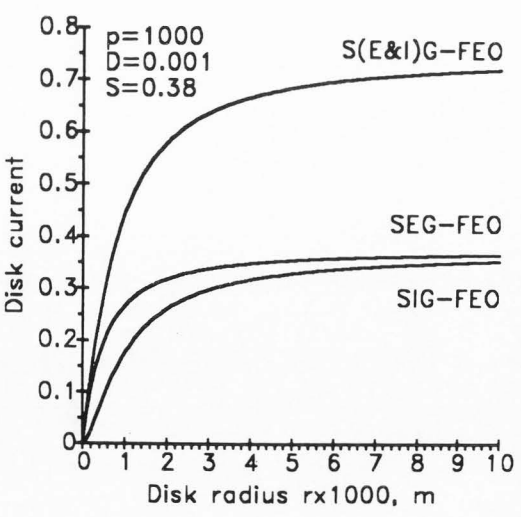

Fig. 7 Total, electron and ion disk currents from the primary ionization of FEO, with the parameters shown.

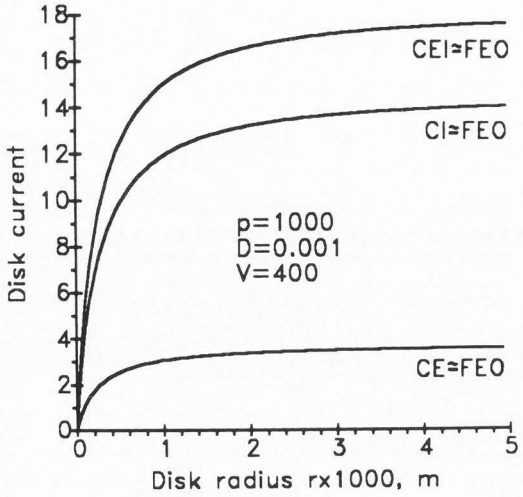

Fig. 8 Total, electron and ion disk currents from the secondary (avalanche) ionization of FEO, with the parameters shown.

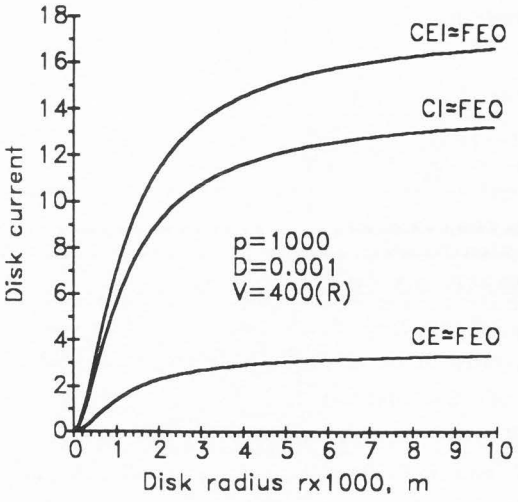

Fig. 10 Total, electron and ion disk current from secondary (avalanche) ionization of FEO, with parameters shown (retarding bias).

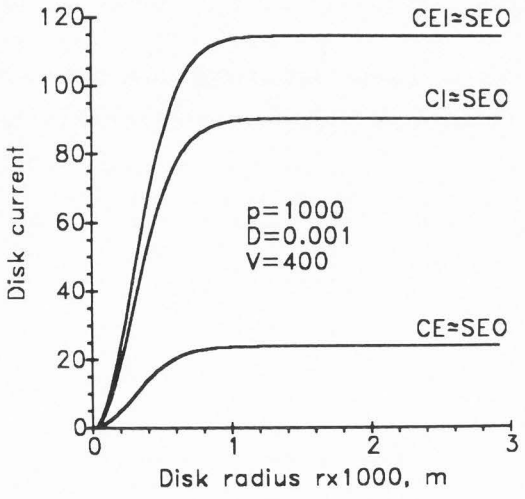

Fig. 9 Total, electron and ion disk current from secondary (avalanche) ionization of SEO, with the parameters shown.

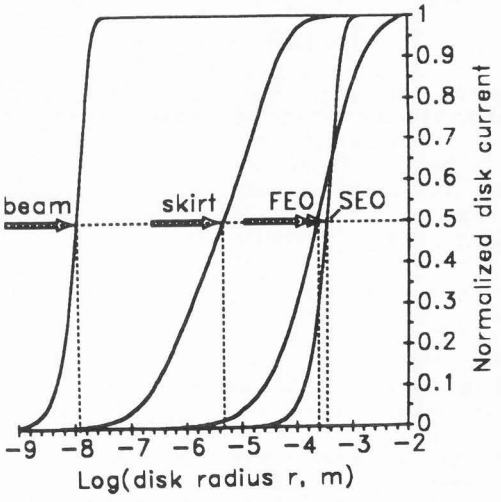

Fig. 11 Simultaneous plot of normalized disk currents for beam, skirt, FEO and SEO (cosine distribution of FEO); dotted lines show the radii at half maximum of current.

found tabulated for values of $\mathscr{E}/p$ only up to 45 V/Pam (Danilatos, 1990b); as $\mathscr{E}/p$ may well exceed this value in the ESEM, an immediate remedy is to extrapolate the available data with the straight line $\varepsilon=36.5+1.73(\mathscr{E}/p)$, but an actual relationship should be established in future work. In all the following examples, to make the comparison easy, we set the beam current and the SEO and FEO coefficients equal to unity, i.e. $I_b=\eta_t=\delta_t=1$.

By use of Eqs. (34), (44) and (49), we obtain the graphs in Fig. 7. We note that the electron current is higher than the ion current and the difference is significant at small disk radius. The total ionization current, i.e. the S(E&I)G-FEO is not very high for this particular FEO distribution and electrode configuration, and it takes place within a few mm of radius.

By applying a bias V=400 volts to the electrodes, we obtain, through avalanche formation, a multiplication of current according to Eqs. (68), (71) and (74) as shown in Fig. 8. We now note that the ion current is much greater than the electron current and the total gain has increased by more than a factor of ten over the initial ionization current.

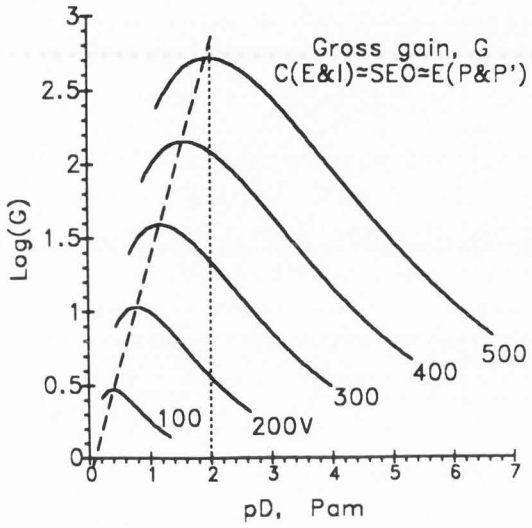

Fig. 12 Logarithm of gross gain versus pD for cascade electrons and ions due to SEO, with different fixed anode bias; dotted line corresponds to m=1.

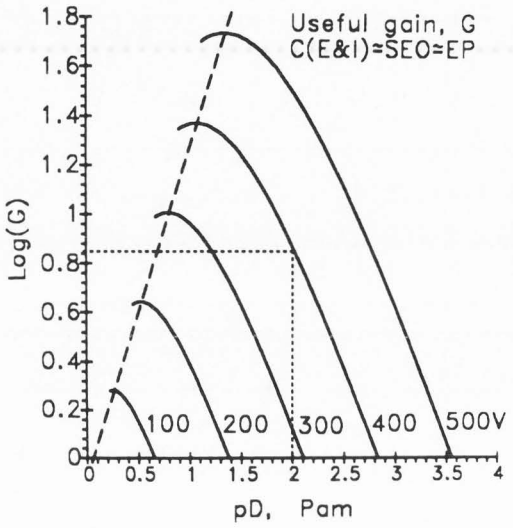

Fig. 13 Logarithm of useful gain versus pD for cascade electrons and ions due to SEO, with different anode bias.

By use of Eq. (51) in conjunction with Eq. (53) for the total current, with Eq. (60) for the electron current and with Eq. (65) for the ion current, we obtain the graphs in Fig. 9. The SEO achieve a relatively high gain of more than two orders of magnitude composed predominantly of ion current. The SEO are distributed and amplified within a small radius of about one mm.

By reversing the applied bias and by use of Eqs. (78), (80) and (82) we obtain the results shown in Fig. 10. The difference from the "forward" biasing is that the distribution is now more spread out in radius.

In order to compare the range of action over radius between various currents, simultaneous plots of the electron probe by Eq. (3) and skirt by Eq. (18), together with results for C(E&I)≃SEO and C(E&I)≃FEO, as above, are shown in Fig. 11. The abscissa shows the logarithm of radius and the ordinate shows normalized values of the functions of disk current obtained by dividing the current by its maximum value at the maximum radius used; at this radius, all currents have reached their saturation maximum, with the exception of C(E&I)≃FEO which, however, for the present FEO distribution, is close enough to its saturation value.

One consequence of the *cosine* form of distribution on the gaseous currents connected to FEO is that these currents approach a finite value, as we increase the electrode radius.

Gross Gain and Useful Gain

The distribution equations for the signals from the specimens, as presented above, refer to the *gross* signal caused by all beam electrons (i.e. those in the skirt and those in the remaining useful probe). To separate the useful signal from the background signal (=noise), these equations must be simply weighted by the appropriate useful gain factors. Below, we calculate the useful gain factors for the SEO and FEO separately.

Slow electrons from object

First we consider the C(E&I)≃SEO≃E(P&P'), which, starting from the specimen surface, multiply according to Eq. (96). For a fixed voltage, this gain depends on the product pD and shows a maximum at some characteristic value of pD. At the maximum we have the Stoletow condition:

$$(pD)_{opt} = \frac{V}{B} \qquad \text{(Stoletow)} \qquad (98)$$

On a Log(G) versus pD diagram, we can easily show that the maxima of gain lie on a straight line:

$$\text{Log}(G)_{opt} = 0.16ApD - 0.16\frac{AV_m}{B}$$

$$\cdots C(E\&I) \simeq SEO \simeq E(P\&P') \qquad (99)$$

Typical curves are presented in Fig. 12 for the case of nitrogen, with V_m=15.5 volts. The curves have been drawn only in the range for which the constants A and B are valid, but they should approach the abscissa asymptotically (i.e. unity gain). There might be little use plotting for values of pD equivalent to m>3, which, for a beam of 10 keV, corresponds to a boundary shown by a vertical line at pD=2. The straight line obeying the Stoletow condition passes close to the origin of the axes.

In order to find the fraction of the gross gain that corresponds to the useful unscattered probe, we must multiply by exp(-m). Taking into account Eqs. (6) and (94), the useful gain is given by

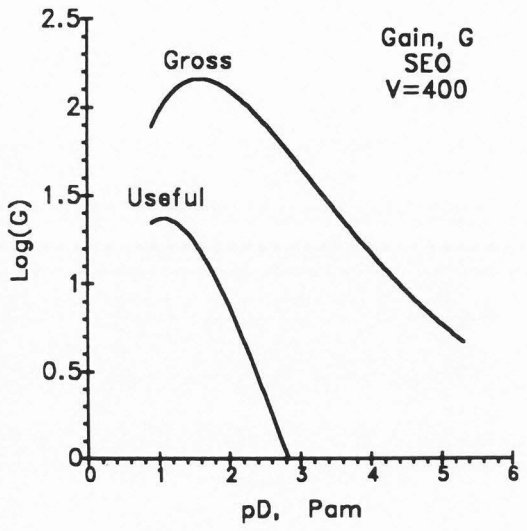

Fig. 14 Simultaneous plot of gross and useful gain for SEO, with 400 volts anode bias.

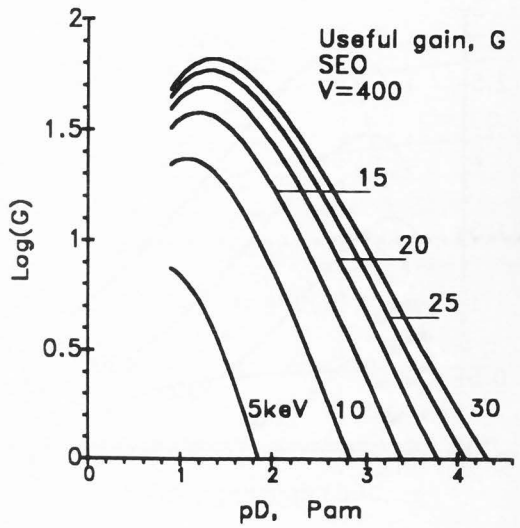

Fig. 15 Logarithm of useful gain versus pD for cascade electrons and ions due to SEO, with different accelerating voltages.

$$G = \exp\left[pD\left(fAe^{-BpD/V} - \frac{\sigma_T}{kT}\right)\right]$$

$\cdots C(E\&I)\simeq SEO\simeq EP \qquad (100)$

A set of curves for the useful gain is shown in Fig. 13. Again, we note a maximum which defines an optimum condition of operation for the ESEM. This new condition is found to be

$$fAe^{-BpD/V}\left(1 - \frac{pDB}{V}\right) = \frac{\sigma_T}{kT}$$

$\cdots$(optimum ESEM operation) (101)

We note that pD and V enter as a ratio in the above equation and, hence, they are proportional to each other. The maxima again lie on a straight line as shown in Fig. 13, because, under the condition of Eq. (101), we obtain a linear relation with respect to pD (pD/V=constant):

$$Log(G)_{opt} = 0.43fAB\frac{pD}{V}e^{-BpD/V}pD$$

$\cdots C(E\&I)\simeq SEO\simeq EP \qquad (102)$

The logarithm of useful gain can, in theory, assume negative values, which means that the gain can be less than unity; however, this may have little practical significance. The curves have only been drawn down to the abscissa. At the previously arbitrary limit of m=3 (where pD=2), we note that the useful gain for a bias V=400 volts is still G=7.1, which is quite significant. In other words, when the beam has lost 95% of its electrons and when using the gaseous detector device (GDD), we may still be able to form acceptable contrast. Therefore, we are led to search for and define yet another practical limit of m, *for the case of GDD*. We could, perhaps, define this limit to be the point where the curve of useful gain becomes unity. Such a limit would, of course, depend on the operating conditions of the GDD.

It is important to compare the overall gain to the useful gain for a fixed voltage, say V=400 volts in nitrogen. This is shown in Fig. 14. The difference between the two curves, due to the skirt, should be kept as low as possible. We note that the two maxima occur at a different pD value, which is fortunate. This implies that, when the ESEM is operating under the optimum condition of Eq. (101), the skirt noise is not yet very high. As pD is increased beyond this point, the difference between gross and useful gain is monotonically increased simultaneously with a decrease of the useful gain, all to the detriment of useful contrast.

We also consider the effect of using different accelerating voltage for the electron beam. A set of useful gain curves with different keV beams is shown in Fig. 15, where the σ_T has been calculated for each keV from Eqs. (16) and (17). It is noted that the effect can be very pronounced. The gain drastically diminishes towards 5 keV (and below), whereas it approaches asymptotically a limiting curve at the high keV range. The limit is simply given by Eq. (96), to which Eq. (100) is reduced, as σ_T becomes very small at very high keV.

If we are interested in the useful gain factors for the signals induced by electrons or ions only, then we must likewise multiply the corresponding gain factors by e^{-m}.

Fast electrons from object

In a similar fashion, we can find the various gain factors associated with the C(E&I)≃FEO. The equations previously derived are applicable for all FEO≃E(P&P'). For the case of a *cosine* distribution of FEO, the gain as obtained with a disk of

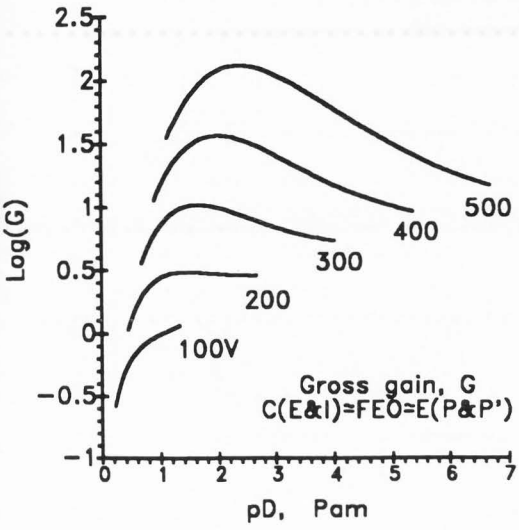

Fig. 16 Logarithm of gross gain versus pD for cascade electrons and ions due FEO, with different anode bias.

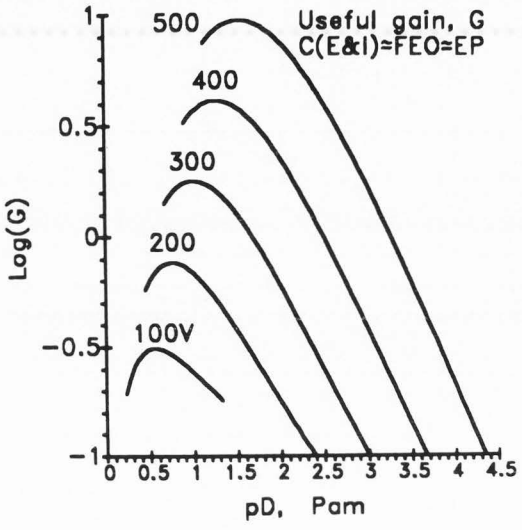

Fig. 17 Logarithm of useful gain versus pD for cascade electrons and ions due to FEO, with different anode bias.

very large radius can be found (after integration) from Eq. (68) as

$$G = \frac{I}{\eta_t I_b} = 2pDS\left[\frac{1}{\alpha D}\left(e^{f\alpha D}-1\right)+1-f\right]$$

$$\cdots C(E\&I)\simeq FEO\simeq E(P\&P') \quad (103)$$

where the correction factor f was accounted for in the limits of integration of Eq. (68) and has been incorporated above for completeness. It can be seen that its effect is small also at low bias, where the gain is mainly determined by the primary ionization by the FEO. At low field, where the avalanche gain is unity, Eq. (103) reduces the same result as Eq. (34) with very large r, i.e.

$$G = 2pDS \quad \cdots S(E\&I)G\text{-}FEO\simeq E(P\&P') \quad (104)$$

which simply states that the gain is proportional to pD and to the ionization efficiency. The gain by Eq. (103) is also proportional to pD, and has a maximum when plotted versus this product. A set of curves using Eq. (103) is shown in Fig. 16. At low bias the curves gradually degenerate to straight lines as per Eq. (104).

By multiplying Eq. (103) by the factor e^{-m}, as previously, we can find the useful gain for C(E&I)~FEO≃EP, and a set of curves is shown in Fig. 17. The curves for V=100 and V=200 volts have less than unity gain (negative values) and have been drawn for completeness. It should be remembered that the equations of gain derived here depend on the distribution function of FEO used, and appropriate adjustments should be made with other distributions.

Uniform FEO Distribution

In a practical situation, the surface of a specimen has variable topography and, as a result, the FEO distribution may change from point to point as the beam scans the image. If this distribution were known for each point of specimen surface, the corresponding ionization function eN(r,h) could be easily established and, then, the various distributions of current could be found exactly as in the case of the cosine distribution. Distributions of special interest are left for future studies; here, the *uniform* (or *spherical*) distribution of FEO will conclude the present investigation. A typical specimen may have such "an average roughness" that a FEO has equal probability in all directions; this is a much more realistic case than the case of a polished specimen. The main functions have been derived for this case and the results are presented below without detailed explanations:

$$\frac{d\eta}{d\Omega} = \frac{\eta_t}{2\pi} \quad (105)$$

$$I(r,D) = \eta_t I_b\left(1-\frac{1}{Q}\right) \quad \cdots FEO \quad (106)$$

$$eN(r,h) = \frac{\eta_t I_b pS}{2\pi(r^2+h^2)} \quad (107)$$

$$I(r,D) = \eta_t I_b pDS\left[\frac{r}{D}\tan^{-1}\left(\frac{r}{D}\right) + \ln Q\right]$$

$$\cdots S(E\&I)G\text{-}FEO \quad (108)$$

$$I(r,D) = \eta_t I_b pDS\left[\frac{r}{D}\tan^{-1}\left(\frac{r}{D}\right)-\frac{1}{2}\left(\frac{r}{D}\right)^2\ln\left(\frac{r}{DQ}\right)+\frac{1}{2}\ln Q\right]$$

$$\cdots SEG\text{-}FEO \quad (109)$$

$$I(r,D) = \frac{1}{2}\eta_t I_b pS\int_0^D \ln\left[1+\left(\frac{r}{h}\right)^2\right]e^{\alpha(D-h)}dh$$

$$\cdots C(E\&I)\simeq FEO \quad (110)$$

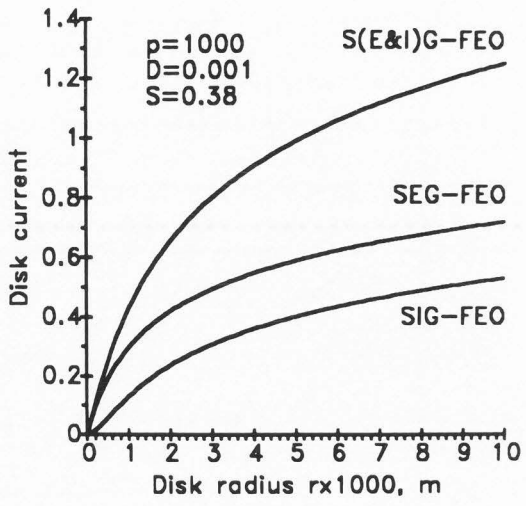

Fig. 18 Total, electron and ion disk current from the primary ionization of FEO, with parameters shown (uniform FEO distribution).

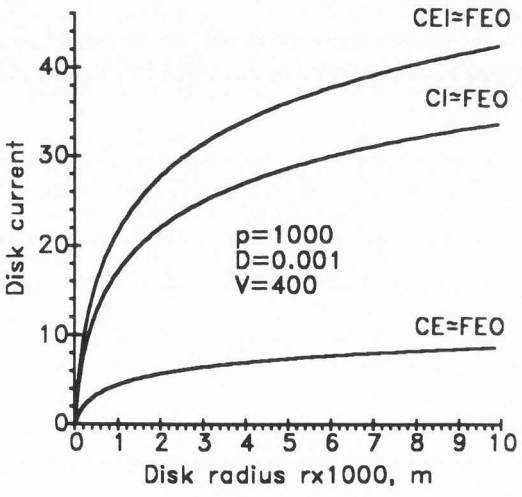

Fig. 19 Total, electron and ion disk current from secondary (avalanche) ionization of FEO, with parameters shown (uniform FEO distribution).

$$I(r,D) = \frac{\eta_t I_b pS}{2\alpha D}\int_0^D \ln\left[1+\left(\frac{r}{h}\right)^2\right]\left[e^{\alpha(D-h)}-1\right]dh$$

$\cdots$CE≈FEO (111)

For retarding field:

$$I(r,D) = \frac{1}{2}\eta_t I_b pS\int_0^D \ln\left[1+\left(\frac{r}{h}\right)^2\right]e^{\alpha h}dh$$

$\cdots$C(E&I)≈FEO (112)

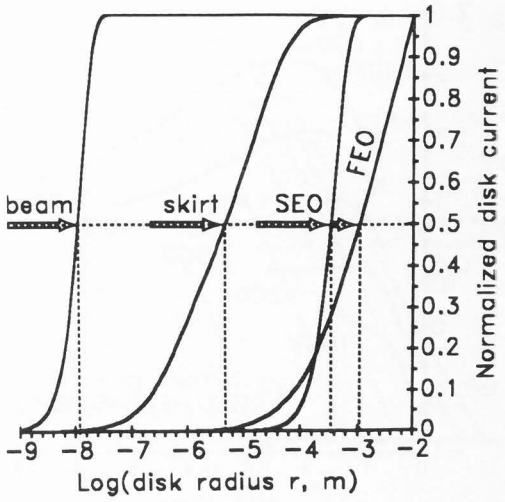

Fig. 20 Simultaneous plot of normalized disk currents for beam, skirt, FEO and SEO (uniform distribution of FEO); dotted lines show the radii at half maximum of current.

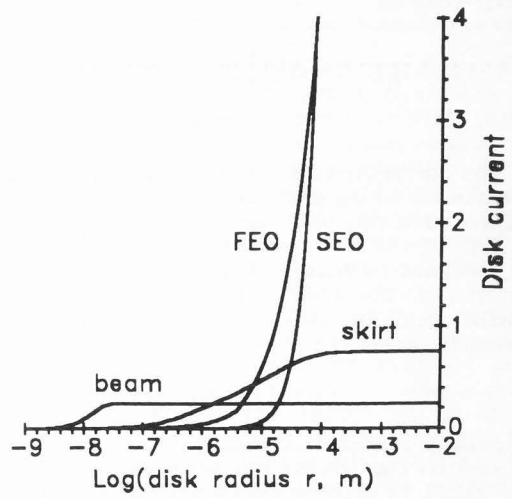

Fig. 21 Simultaneous plot of disk currents for beam, skirt, FEO and SEO (cosine distribution of FEO).

$$I(r,D) = \frac{\eta_t I_b pS}{2\alpha D}\int_0^D \ln\left[1+\left(\frac{r}{h}\right)^2\right]\left[e^{\alpha h}-1\right]dh$$

$\cdots$CE≈FEO (113)

We can visualize the results for this new distribution in the following graphs. The same operating conditions have been chosen as previously. Fig. 18 shows the primary ionization currents by the FEO as determined by Eqs. (108) and (109); the positive ion current component was simply derived from the difference between the total and

the electron current. We note that now the ionization is spread outwards with no indication of a saturation level. The electron component is higher than the ion component and the total current has increased well above that given by the cosine distribution.

The corresponding graphs for Eqs. (110) and (111), with external bias V=400 volts, are shown in Fig. 19. The gaseous gain is considerably increased, well above that derived by the cosine distribution. A similar result (not shown) is found with a retarding field, in which case the corresponding current values are below those with a forward field.

It is important to compare the range of action of various currents for the uniform distribution, as was done in Fig. 11 for the cosine function. The result is shown in Fig. 20. The range of C(E&I)≃FEO is now well beyond the range of C(E&I)≃SEO. The actual value of C(E&I)≃SEO is much higher than the corresponding value of C(E&I)≃FEO within the range of the former, except for extremely low values of the radius. The cross-over point between the two curves in Fig. 20 (as in Fig 11) is artificial, because of the normalization procedure and because an arbitrary maximum value that is not a saturation value was used for the C(E&I)≃FEO. A more realistic situation is shown in Fig. 21 without normalization. The true cross-over point would be obtained by using the real values for δ_t and η_t.

Equations of Charge Conservation

In the vacuum specimen chamber of the conventional SEM the charge conservation is expressed by the well known equation

$$I_b = I_F + I_S + I_O \qquad (114)$$

where $I_b \equiv I\{EP\}$ is the incident beam current, $I_F \equiv I\{FEO\} = \eta_t I_b$ is the current of "backscattered electrons", $I_S \equiv I\{SEO\} = \delta_t I_b$ is the current of "secondary electrons" and I_O is the "absorbed" current by the specimen (object).

The appropriateness of the term "absorbed" has been questioned in view of the signal induction mechanism (Danilatos, 1990b; 1990c). Let us consider the following *gedanken* experiment: The specimen under examination is a 100% insulating membrane enveloping a metal conductor that is connected to the image recording system of an SEM. The electron beam scans only a single raster on the specimen surface with a minimum current, so as it is not appreciably deflected by the deposited charge on neighboring scanning lines. The minimum current is supposed to be sufficient to produce satisfactory signal-to-noise ratio. Then an image will be recorded by the system without the deposited charge actually being "absorbed" by the specimen (i.e. the insulator). The signal pulses are generated *by induction during the flight* of the electrons *prior* to the termination of their motion. The image thus recorded would carry the genuine information about the specimen, as the beam scans a virgin surface for the first time, before any beam irradiation artifacts have occurred. The practicality of such an experiment may be questioned on account of the actual levels of current required and the available hardware of the SEM (e.g. pre-focusing requirement). However, this experiment demonstrates that the absorption per se is not a principal prerequisite for image formation. Absorption is rather a necessity to avoid continuous charge accumulation and accompanying problems. In the ionized gaseous environment of ESEM, charge accumulation is effectively suppressed, and imaging of insulating materials is commonplace with all main imaging modes. In the above context, the word "absorbed" becomes redundant, but the term "specimen" or "object" current may still be retained to refer to the amount of charge deposited as per Eq. (114).

In the ESEM, we have seen that additional components of current flow in the system on account of the ionization in the gas by various sources. Therefore, Eq. (114) must be modified by adding a term for the total ionization current I_I:

$$I_b + I_I = I_F + I_S + I_O + I_I \qquad (115)$$

The ionization term is composed mainly of three partial terms:

$$I_I = I_{bI} + I_{FI} + I_{SI} \qquad (116)$$

where I_{bI} is the ionization caused by the incident beam, I_{FI} that by the fast electrons from object and I_{SI} that by the slow electrons from object. We can easily find these terms from the corresponding equations by taking the limit at very large radius. This can be done for I_{bI} and I_{SI}; a limit is predicted for I_{FI} with the cosine distribution of FEO, but not for the uniform distribution. Naturally, there is always a limit, because the FEO can only travel a finite distance, as they ultimately dissipate all their energy, but after a number of collisions, the conditions for the equations are no longer valid. Thus, we specifically have:

$$I_{bI} = \frac{I_b pS}{\alpha}\left(e^{\alpha D} - 1\right) \qquad (117)$$

$$I_{SI} = \delta_t I_b \left(e^{\alpha D} - 1\right) \qquad (118)$$

$$I_{FI} = \frac{2\eta_t I_b pS}{\alpha}\left(e^{\alpha D} - 1\right) \quad \cdots \text{cosine distribution} \qquad (119)$$

The ionization current is taken to be positive with "forward" bias, and negative with SEO-retarding bias; in the latter case, we may have $I_{SI}=0$.

The ionization currents can extend well beyond the physical size of a specimen and can be collected by a system of electrodes placed below, on the side or above the specimen. Therefore, the

meaning of the word "specimen" current is now questioned for a different reason. However, we may retain this term, if we redefine the meaning of the word "specimen" (or "object"); we may define it to be, first of all, that portion of the specimen that is actually imaged, but, to be consistent with the new terminology introduced, it is preferable to define as specimen that portion of the specimen that is struck by all electrons in the probe and the skirt together, i.e. by E(P&P'). Then, the term I_0 may be retained with its previous meaning as in Eq. (114). By combining Eqs. (114) and (115) and rearranging terms, we get

$$(I_b - I_{bI}) = (I_F + I_{FI}) + (I_S + I_{SI}) + (I_O - I_I) \qquad (120)$$

By setting $I_{bbI} \equiv I_b - I_{bI}$, $I_{FFI} \equiv I_F + I_{FI}$, $I_{SSI} \equiv I_S + I_{SI}$ and $I_{OI} \equiv I_O - I_I$, we finish up with an equation having the same form as the equation of charge conservation in vacuum:

$$I_{bbI} = I_{FFI} + I_{SSI} + I_{OI} \qquad (121)$$

In the light of the present analysis, the use of the conventional "specimen absorbed" current (I_0) with "wet" specimens, and the "deterioration" of image by the ionization of the gas, as understood by Shah and Beckett (1979) and by Shah (1987), should be reappraised.

The precise mechanism of charge dissipation in the ESEM, and how it affects the contrast and image formation, constitutes a separate topic outside the scope of this paper. Early works on charge neutralization have been reported by Moncrieff et al. (1978) and Crawford (1979).

Discussion

The theoretical analysis of charge distribution presented above yields fundamental information useful in the design of the GDD, in the studies of charge dissipation and generally in the overall operation of ESEM. Through the interplay of various parameters one can manipulate a desired result. The many possibilities will not be covered in this discussion, but a few points will be highlighted.

One important point of this investigation is that it can provide a quantitative explanation for some of the observed transitions of contrast when the pressure, specimen distance and electrode radius is varied (Danilatos, 1983; 1988; 1990b; 1990c). The SEO can be confined within a small radius, and because their amplification far exceeds that of the FEO, the image will show information predominantly relating to the SEO. The SEO originate from the top layer of the specimen and they may be SEO-EP or SEO~EP and so on; the known rules of contrast and resolution are also applicable to the ESEM. By use of an annular electrode outside the range of SEO, one can detect purely FEO contrast.

A rather unexpected result is that the FEO lie above the SEO signal in the very small radius region; in the example of Fig. 21, this radius is about 40 μm. The absolute value of signal is low, but still detectable. The practical significance of this is yet to be explored by amplifying the signal above a suitably chosen pressure limiting aperture (PLA). Imaging with an electrode placed above the PLA has already been achieved and the theoretical groundwork has been reported elsewhere (Danilatos, 1990a; 1990b).

The positive ions contribute a major component to the signal induced and they can play a limiting role in the frequency response of the GDD. This has been discussed in more detail elsewhere (Danilatos, 1990b).

The main theoretical results shown in this paper are in general qualitative agreement with all experimental evidence accumulated to date. It might appear an easy task to quantitatively demonstrate by experiment the equations derived in this paper, as, indeed, concentric annular electrodes have already been tested in the ESEM (Danilatos, 1990c). However, a strict quantitative comparison between experiment and theory may be futile on account of significant uncertainties with some parameters of the equations. One such uncertainty relates to the α-coefficient, which strongly depends on the purity of gas. This parameter has involved several decades of work, the intricacies of which can be found in widespread publications.

The parameter ε is also critical. This not only depends on the gas composition, but, in addition, the data available are not in the range of E/p mostly of interest in the ESEM. What is known is mainly found in early works of this century. In the present paper, only a crude extrapolation was used based on one of these early works.

Another parameter is the scattering cross-section. The equations used are reliable, except they themselves rely on the precision of other parameters, a critical one being the atom radius, here calculated by Eq. (15). The ionization scattering cross-section and the associated ionization efficiency are also important. Multiple-backscattering of FEO between the electrodes can have a significant effect on S.

One has to exercise special care with the remainder parameters in an experimental set-up, but the determination of the above-mentioned parameters for the conditions of ESEM is a necessary prerequisite, before we proceed to quantitatively verify the present equations. Such work is, of course, outside the scope of this presentation and is left for the future. The ESEM is, in fact, a new precision instrument which can be used for the determination of these parameters and some of the classical experiments of ionization physics can be redesigned in the actual conditions of the instrument.

It should be noted that both the loss of electrons from the electron probe and the gaseous gain contain an exponential term, which, for a small variation of pressure, distance, accelerating voltage etc., results in a significant variation of gain, useful signal, noise etc. The examples presented mainly serve to demonstrate the theory and should not be taken as an indication of the ultimate limits of the GDD. In fact, a rough comparison with experience shows that better results are obtained in reality, and the numerical values of the examples presented are likely to err on the safe side (i.e. they are conservative).

However, the present theory can be relied upon to further plan experiments to explore and improve the performance of ESEM.

Conclusion

After the focused electron beam enters in the high pressure conditions of the ESEM specimen chamber, it results in a host of distinct distributions of electron currents. The primary beam continuously loses electrons, as it approaches the specimen, but is left with sufficient current and the same distribution as in the original (i.e. in vacuum) spot, to permit imaging with the original resolving power. For practical purposes, the single scattering theory has been used to derive relatively simple equations for the surrounding electron skirt composed of the scattered electrons and extending over a radius of tens of microns. All the slow electrons from the specimen surface can be confined within a small radius, whereas the fast electrons usually extend beyond this radius. A separation of the two types of signal is possible either with suitable electrode size and bias, or with a reversal of the bias to suppress the slow electrons from the specimen. All these currents together with the charge density in the bulk of the gas can be described with appropriate equations. Equations relating to the FEO ionization have been derived for the cases of cosine and uniform distributions of FEO; similar steps can be followed for other distributions of interest. The present investigation fulfills one of the tasks for future work, as set out in a previous report (Danilatos, 1990b).

Acknowledgement

The support by Electroscan Corporation is gratefully acknowledged.

List of Symbols

a_H Bohr radius
A gas constant, or see Eq. (13)
B gas constant
c standard deviation
D separation of parallel disk electrodes
D_m minimum effective ionizing distance
$\frac{d\sigma}{d\Omega}$ differential cross-section
$\frac{d\eta}{d\Omega}$ differential FEO coefficient
$\frac{d\sigma_e}{d\Omega}$ elastic differential cross-section
$\frac{d\sigma_i}{d\Omega}$ inelastic differential cross-section
e electron charge
E beam accelerating voltage, FEO energy
E_b incident electron beam energy
f correction factor
$f(\theta)$ scattering amplitude
$f_e(0)$ electron scattering amplitude at $\theta=0$
G gain factor
h, or h' distance from bottom electrode
I_b incident beam current in vacuum
I_{bI} beam ionization current
I_F FEO current
I_{FI} FEO ionization current
I_I total ionization current
I_n negative (electron) current
I_o object current
I_p positive (ion) current
I_S SEO current
I_{SI} SEO ionization current
J ionization energy of gas
j(r,D) current density at point (r,D)
J(r,D) disk current within radius r
k Boltzmann constant
L_i ionization mean free path (for electrons)
m average number of collisions per incident beam electron
n density of gas particles
N(r,θ), or N function of primary ionization rate
p gas pressure
q charge
Q see Eq. (27')
r radial distance from system axis
r_1, r_2 radii of annular electrode
R atom radius
$\vec{R}_0$ unit position vector
s ionization efficiency coefficient
S, or S(E) ionization efficiency
T absolute temperature
V_m minimum effective ionizing potential
V(r) single-scattering probability distribution for electrons
$W=E/E_b$
z travel distance from PLA
Z atomic number
α first Townsend coefficient
δ_t total SEO coefficient
ε ratio of electron to gas molecule energies
$\mathcal{E}$ intensity of electric field
η FEO coefficient
η_t total FEO coefficient
θ scattering angle
θ_E see Eq. (12)
θ_0 see Eq. (11)
λ electron wavelength
λ_n linear negative (electron) charge density
λ_p linear positive (ion) charge density
ρ reduced radius, or charge density
ρ_n negative (electron) charge density
ρ_p positive (ion) charge density
σ_T total electron scattering cross-section of a gas particle
Σ cumulative probability
υ velocity
υ_n negative (electron) charge velocity
υ_p positive (ion) charge velocity
Ω solid angle

Table of Abbreviations

CE cascade electrons
CI cascade ions
C(E&I) cascade electrons and ions
E electron
EP electron(s) (from) probe
EP' electrons from scattered probe (i.e. skirt)
E(P&P') electrons from probe and skirt
ESEM environmental scanning electron microscope(y)
F fast
FEO fast electrons from object
G gas
GDD gaseous detection (or detector) device
I ion
L light
O object
P probe
P' scattered probe
PLA pressure limiting aperture
R rays
S slow
SEO slow electrons from object
SEG slow electrons from gas
SIG slow ions from gas
(S&F)EG slow and fast electrons from gas
S(E&I)G slow electrons and ions from gas
W walls
X x-rays
- directly caused by
~ indirectly caused by
≃ directly and indirectly caused by

References

Burge RE, Smith GH (1962) A new calculation of electron scattering cross-sections and a theoretical discussion of image contrast in the electron microscope. Proc. Phys. Soc. 79, 673-690.

Cobine JD (1941) Gaseous Conductors. McGraw-Hill, New York and London, 81.

Corson DR, Wilson RW (1948) Particle and quantum counters. Rev. Sci. Instr. 19, 207-233.

Crawford CK (1979) Charge neutralization using very low energy ions. Scanning Electron Microsc. 1979; II: 31-46.

Danilatos GD (1983) A gaseous detector device for an environmental SEM, Micron and Microscopica Acta 14, 307-318.

Danilatos GD (1988) Foundations of environmental scanning electron microscopy. Adv. Electronics Electron Phys. 71, 109-250.

Danilatos GD (1990a) Design and construction of an environmental SEM (Part 4). Scanning 12, 23-27.

Danilatos GD (1990b) Theory of the gaseous detector design in the ESEM. Adv. Electronics and Electron Phys. 78, 1-102.

Danilatos GD (1990c) Mechanisms of detection and imaging in the ESEM. J. Microsc. (in press).

Engel A von (1965) Ionized Gases. Oxford at the Clarendon Press, 63.

Huxley LHG, Zaazou AA (1949) Experimental and theoretical studies of the behavior of slow electrons in air. Proc. Roy. Soc. London 196, 402-426.

Jost K, Kessler J (1963) Die Ortsverteilung mittelschneller Elektronen bei Mehrfachstreuung (The spatial distribution of medium-energy electrons during plural scattering). Zeits. Phys. 176, 126-142.

Lenz F von (1954) Zur Streuung mittelschneller Elektronen in kleinste Winkel (Scattering of medium-energy electrons in very small angles). Zeits. Naturforsch. 9a, 185-204.

Massey HSW (1969) Electronic and Ionic Impact Phenomena. Vol. 2, Oxford Clarendon Press, 667, 972.

Matsukawa T, Shimizu R, Hashimoto H (1974) Measurements of the energy distribution of backscattered kilovolt electrons with a spherical retarding-field energy analyzer. J. Phys. D: Appl. Phys. 7, 695-702.

Moncrieff DA, Barker PR, Robinson VNE (1979). Electron scattering by gas in the scanning electron microscope. J. Phys. D: Appl. Phys. 12, 481-488.

Moncrieff DA, Robinson VNE, Harris LB (1978) Charge neutralization of insulating surfaces in the SEM by gas ionization. J. Phys. D: Appl. Phys. 11, 2315-2325.

Peters K-R (1982) Conditions required for high quality high magnification images in secondary electron-I scanning electron microscopy. Scanning Electron Microsc. 1982; IV: 1359-1372.

Reimer L (1985) Scanning Electron Microscopy. Springer-Verlag, Berlin, 138.

Shah J (1987) Electron microscopy comes to life. Spectrum No. 208, 6-9 (Central Office of Information, London).

Shah JS, Beckett A (1979) A preliminary evaluation of moist environment ambient temperature scanning electron microscopy. Micron 10, 13-23.

Townsend JS, Tizard HT (1913) The motion of electrons in gases. Proc. Roy. Soc. A: London 88, 336-347.

Weston GF (1968) Cold Cathode Glow Discharge Tubes. London ILIFFE Books Ltd. London, 3.

Discussion with Reviewers

A. Dubus: Could you briefly comment on the advantages of ESEM with respect to SEM?

Author: The presence of a gaseous atmosphere around the specimen has the following general advantages: It maintains a moist environment so that wet specimens do not dry out, dynamic changes and interactions between solid/liquid/gas phases can be monitored in situ, including experiments on gas flow and gas dynamics in situ. The gas becomes ionized and hence a good electrical conductor, which eliminates the need for treatments of insulating specimens such as coatings, chemical treatments, or use of some very low accelerating voltage (with limited abilities). The gas, apart from its conditioning properties can also act as a detection medium or as a generalized gaseous detection device; this has ushered some unique and novel possibilities of detection and imaging techniques for electron microscopy in general. The true surface properties of practically any specimen can be examined under a variety of detection modes. Many preparation techniques have become redundant, resulting in simplicity, time saving and ease of operation. However, many known preparation

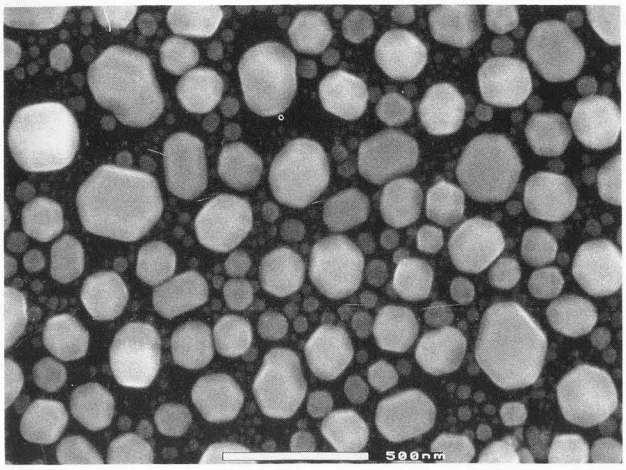

Fig. 22 Gold particles on carbon placed 1 mm from PLA at 1133 Pa pressure of water vapor and 30 keV. The smallest particles discerned are less than 10 nm (courtesy of Electroscan).

techniques may be used in different combinations or even novel techniques may be devised to allow new applications in the ESEM. As the gas pressure can be varied from high vacuum up to room atmosphere (the maximum pressure is determined by the particular design of ESEM and the particular application) the ESEM inherits all the conventional advantages of SEM with the addition of a new dimension. The ESEM and SEM are not competing with each other, they are not two separate alternatives, or one should not be seen versus the other: ESEM is simply the natural extension of SEM.

A. Dubus: You developed fully analytical calculations for ESEM. Do you think that a Monte-Carlo simulation could help you in understanding the whole problem of signal formation in ESEM?
Author: Yes. The analytical method has yielded some very simple expressions to be used for our understanding of the most fundamental properties of the system at this early stage of ESEM developments. For more refined calculations, where the analytical approach becomes extremely complex, the Monte-Carlo method could be very helpful. However, many useful derivations here are based on a detailed understanding of physical processes which cannot be simply substituted by Monte-Carlo proceedings.

J.M. Cowley: As is the case with solids, there will presumably be some small-angle (10^{-3} rad or less) inelastic scattering from electronic excitation in the gas molecules. To what extent will this affect the resolution of the ESEM?
Author: It is true that the small angle inelastic scattering is also present in gases. This has been taken into account during the calculations of beam profiles by use of the Jost and Kessler method (Danilatos, 1988) but no visible effect was found, a fact that was further confirmed also by experiment. In addition, the included micrograph (Fig. 22) shows no loss of resolution with a test specimen in the presence of gas. With visible details below 10 nm and a specimen-PLA distance of one mm, electrons scattered within angles down to 10^{-5} rad have no noticeable effect. Therefore, the limit of resolution in gas is determined only by the available spot diameter which is the same as in vacuum.

K.-R. Peters: You assume that the origins of P and P' are similar and, for theoretical reasons, lie in one point. In Fig. 21, how would the current radius of different signals change if a skirt radius of several mm would be encountered?
Author: In practice, if the skirt radius is increased from the assumed tens of microns to several mm, then the distance of the specimen from the PLA as well as the dimensions of the electrodes would also increase in the same proportion, so that the origin of P' may still be assumed as a point. If, however, we wish to calculate the various distributions within a radius comparable to the radius of the skirt, then the equations are no longer valid. The analytical method would become quite complex, and Monte-Carlo calculations should be in order.

K.-R. Peters: Cascade amplified slow electrons can be collected at any take-off angle with small electrodes positioned appropriately. Is it possible to separate on tilted specimens the CSE-FEO signal produced by low-loss electrons from a CSE-SEO signal?
Author: In principle, yes. The practical ease or difficulty can only be determined by careful experimentation.

K.-R. Peters: Why is the gaseous detection device conventionally used with positive bias only? Under which conditions (type of specimen, gas pressure etc.) and for which signals would the negatively biased detector provide better S/N ratio?
Author: If by the word "conventionally" you mean the existing commercial type of ESEM available at present, then, I presume, it is for standardization and manufacturing requirements reasons that only positive bias is used. The present author has reported results by use of both positive and negative bias since 1983. A sufficient negative bias would suppress the SEO and allow only the FEO to ionize the gas and be detected (the x-rays and other photons are not considered here). This case is described by the equations in the section for SEO-retarding field. The S/N ratio would then be determined by the FEO mode of detection with the known rules. With reversed bias, the slow electrons liberated by the action of FEO on the top electrode (SEW≈FEO, i.e. converted backscattered electrons) will result in additional electron avalanches propagating from the top electrode to the bottom electrode. The increased gain will contribute towards an improved S/N ratio within the FEO mode of detection alone.

K.-R. Peters: Is it possible to use differently shaped collection field gradients (formed by elec-

trostatic or electromagnetic lenses) to separate the CSE-O signal from the CSE-FEP and the CSE-FEP' signal?
Author: In principle, yes, but in practice, complete separation may prove very difficult, even impossible. As both EP and EP' ionize the gas along their entire length, the cascades originating in the gas close to the specimen surface, will have distributions comparable to those originating from SEO (with positive bias). With regard to FEO mode alone, the background noise caused by S(E&I)G-E(P&P') can be simply eliminated by an annular electrode placed outside the radial range of this noise.

What seems to be very difficult to rid of is the noise generated by the skirt-specimen interaction. Only under special electrode configurations, this may be possible to reduce.

M. Kotera: How the inelastic scattering cross-section (Eq. 10) is obtained? If it includes all kinds of inelastic processes, would you comment on its applicability?
Author: The inelastic cross-section was derived by Lenz (1954) and further adapted and discussed by Jost and Kessler (1963) and Danilatos (1988). It includes all kinds of inelastic processes incorporated in the "ionization" energy J of the gas (see Eq. 12). The problem is that this coefficient is not universally established and, hence, the accuracy for the inelastic cross-section is largely dependent on the accuracy of the chosen value for this coefficient. In the present examples calculated, it has been taken equal to the first ionization potential for atomic nitrogen or argon. If needed in future work, these calculations should be repeated with a more realistic value of J for each gas.

K.-R. Peters: At high vacuum, specimen current contrast images are possible only on electrical conductors. However, voltage contrast images can be produced on insulators as well as conductors. Is it possible to generate voltage contrast images in the ESEM?
M. Kotera: Because of charge neutralization process at the specimen surface, the voltage contrast, which is observed by the SEM, might not be visible by the ESEM. Is it true?
K.-R. Peters: On smooth insulators, the surface charge is neutralized by attracted charge carriers provided by gas ionization but the depth charges remain. Do you see any possibility to image the depth charge distribution in the ESEM?
M. Kotera: Although the ESEM does not show a severe charging-up problem even at insulating materials, incident primary electron produces a strong electric field inside the specimen, and the charging effect should still show in the images of the ESEM. Does it happen in your experiment?
Author: First of all, the voltage contrast observed on insulators with SEM in vacuum is limited only to certain types of specimens or to specific beam accelerating voltages and conditions. The insulating specimen area under observation should be such as not to allow excessive charging that would make imaging, in general, problematic. It is an experimental fact that such problematic charging is not present in the ESEM, hence, imaging is possible with all insulators under a variety of conditions (gas pressure, accelerating voltage etc.). When we say that charging artifacts are suppressed, we do not necessarily imply, or say, that charging is totally eliminated, i.e. all beam deposited charge is neutralized. No controlled experiments have been carried out to measure this effect. However, from the dramatic variations of contrast that have been observed on insulators as the gas pressure is varied, it may be inferred that voltage contrast is possible to exist under certain operating conditions. Depth charging and conduction in insulators and charge neutralization in the ESEM are topics yet to be explored. We cannot definitely answer these questions, but it is hoped that the present work will help their further investigation.

D. Newbury: Please explain the induction mechanism of signal generation, since at least one of the critical references (1990c) is "in press". In the gedanken experiment discussed in the manuscript, it is not obvious to me why "an image will be recorded without the deposited charge actually being 'absorbed' by the specimen". A more detailed explanation is needed in that discussion.
Author: While a charge is in motion between two electrodes connected through an external circuit, a current given by Eq. (35) flows through the external circuit. When the charge arrives at the electrode, no further current flows. As the electron beam scans over a virgin pixel, both the *incident* beam electrons and the electrons *leaving* the specimen induce pulses during their flights. The sum total of all pulses is the signal detected from that pixel, while a net charge has been deposited on the surface. If the surface is an insulator and an electrode is placed some distance below the specimen surface, a signal will be induced onto the electrode, without charge having to flow though the insulator (which is a dielectric). In reality, a current will flow though the insulator sooner or later. The electrical properties of the specimen will determine the speed by which the deposited charge is absorbed through the insulator. This may or may not have an appreciable effect on the image, depending on various parameters of the system. However, these effects are after-effects and are not described by our gedanken experiment which assumes an ideal insulator. Thus, an image can be recorded without the electrons actually flowing though the specimen.

K.-R. Peters: The "induction contrast" refers to variations of charge carrier transport between the electrode of the gaseous detection device and its reference electrode. However, the same device will also collect CSE providing for a "collection contrast" component which refers to the number of collected charge carriers. The interesting concept may provide a base for an experimental design for separation of the slower moving ion signal from their faster moving electron signal counterparts. Under which circumstances (type of specimen and operation conditions) will both contrast components be equal or different?
Author: Throughout this work, equations have been derived for the electron and ion currents sepa-

rately. For example, Fig. 9 shows the intensity of each component and we note that the ions are predominantly responsible for the signal detected. However, this is not always the case, because it is possible, by use of particular electrode configurations, to filter the ions out and use only the electrons. The complete answer to your question goes beyond the limits of this presentation and could constitute the subject of further reporting.

It is not clear why you introduce "induction contrast" and "collection contrast" terms. One can say that the contrast with an ionization GDD is due only to induction and that the "collection" (i.e. counting) of charges may only lead to an incorrect signal intensity.

D. Newbury: What is the effect of the use of a gas such as water vapor, which in addition to being ionized can presumably form both positive and negative ions (H^+ and OH^-)?

Author: When the external field is sufficiently strong, the concentration of the negative ions H_2O^- is expected to be very small in comparison with the free electrons and, thus, any effect on the frequency response and various distributions should be insignificant. At low external fields, we can expect to have high concentrations of H_2O^+ and H_2O^-, since the electron attachment probability with water molecules is relatively high. The concentration of the negative ions OH^- is not known, but, with the kilovolt range of the ESEM, this should be low. In cases where the OH^- and H^+ ions are significant in numbers, both the distribution and frequency response would be modified in a way predicted by the equations provided. We need to know the corresponding drift velocities and ionization efficiency of the process.